Scanning-tunneling-microscope study of antiphase domain boundaries, dislocations, and local mass transport on Au(110) surfaces

J. K. Gimzewski,* R. Berndt, and R. R. Schlittler
IBM Research Division, Zurich Research Laboratory, 8803 Rüschlikon, Switzerland
(Received 17 May 1991; revised manuscript received 4 November 1991)

We have used a scanning tunneling microscope to investigate surface defects and atomic motion occurring on Au(110)(1×2) reconstructed surfaces at room temperature over a period of time of several hours. Evaluation of time-lapsed topographies shows that distinct changes occur at step structures and domain walls. These features can be classified into basic building blocks to model surface disorder and from the relative changes occurring at each element a local description of mass transport is obtained. Local transport via kinks occurring along atomic rows of the superstructure in [1$\bar{1}$0] is observed to dominate. Finally, unique atomic structures introduced by bulk dislocations are presented and the subsequent influence on the creation of new phase boundaries and distortions in the surface superstructure are discussed.

I. INTRODUCTION

All low-index gold surfaces exhibit a tendency to increase their atomic surface density through reconstruction.[1] For the (110) surface, this is achieved by means of the formation of (111) microfacets resulting in a closely packed surface with lower surface energy than the (1×1) surface despite the increase in microscopic geometric area.[1] The lowest-order possibility of such microfaceting is the (1×2) reconstruction in which alternating atomic rows in the [1$\bar{1}$0] direction are removed. A variety of techniques [low-energy electron diffraction (LEED),[2–4] atom scattering,[5–7] high-resolution electron microscopy,[8] scanning tunneling microscopy (STM),[9,10] x-ray,[11] and medium-energy ion scattering[12,13] have established the existence of the "missing-row" model and, in addition, showed that the outermost gold layer is relaxed inwardly by some 20% of the bulk atomic layer spacing.

Theoretically the missing-row structure has been favored by tight-binding[14] and pseudopotential density functional calculations[15] as well as by a calculation using a semiempirical "glue" Hamiltonian.[1] The latter model predicted that higher-order reconstructions such as (1×3) or (1×4) would be energetically similar. Wolf, Jagodzinski, and Moritz[16–19] published an extensive study on the nature of surface disorder to account for the diffuseness of LEED spots in the [001] direction which is observed already at room temperature and increases with temperature transforming at 420 °C into a diffuse (1×1) LEED pattern. Here, one-dimensional disorder was modeled by assuming strictly ordered chains along the [1$\bar{1}$0] direction. Binnig *et al.*[9] were the first to provide real-space images of this disorder using scanning tunneling microscopy. They observed a heavily disordered surface formed by (1×3) reconstruction randomly interspersed with the (1×2) phase. More recent STM studies where the clean surface was annealed at ~300 °C for periods of time exceeding 6 h followed by quenching to room temperature resulted in ordered terrace lengths of 8–20 nm along the [001] and >100 nm along the [1$\bar{1}$0] directions, respectively,[20] in agreement with our preliminary observations.[21] A similar anisotropy in step structure was observed on the Pt(110)(1×2) reconstructed surface.[10]

While the geometric arrangement of atoms on the Au(110) surface has been thoroughly studied, less information on self-diffusion of this surface is available. Using STM, Jaklevic and Elie[22] observed annealing of craters in Au(111) generated by tip-surface contact. These craters were a few atomic layers deep and had a volume of some 1000 atoms. Jaklevic and Elie were able to identify surface self-diffusion as the dominating process and estimated rates for a number of atoms filling up the craters but could not resolve individual atoms. Emch *et al.*,[23] in their study of epitaxial gold films with STM in air, observed that terrace edges move at speeds in a wide range (0.05–5 Å/s). Lin and Chung[24] attempted to extract an activation energy from STM measurements of profile decay of annealed polycrystalline gold films. Despite these encouraging results, to date the influence of local atomic structures on surface diffusion processes, in particular the role played by defects, remains unresolved.

In this paper we present a detailed investigation of the atomic nature of "disorder" on the Au(110) surface. In particular, we show that surface structures are formed by two principal types of antiphase domain boundaries. The evolution of these structures with time is clarified by several time-lapse sequences of atomically resolved STM images. In diffraction measurements, ordered domains must be larger than the coherence length in order to observe sharp diffraction patterns. On the other hand, previous STM measurements have indicated that these domains are often too small to fulfill this condition. Our measurement of large scan areas demonstrates that the statistical nature of diffraction measurements and the local nature of STM can be brought into harmony by visualizing antiphase domain distributions, on large scale

 ©1992 The American Physical Society

images. A distinct anisotropy in step distribution and structure was found in $[1\bar{1}0]$ and [001] with evidence of step bunching in [001] but with the absence of step coalescence into (111) facets. Our STM observations also indicate the temporally unstable nature of the Au(110) surface where surface diffusion results in a constantly changing distribution of antiphase domains. The antiphase boundaries themselves form a variety of patterns of (1×2) domains whose structure may be understood in terms of basic atomic building blocks. An analysis of the topographs in the framework of such a model gives a deeper insight into which particular atomic configurations exhibit greatest mobility and hence less local stability of the surface. We suggest that the relative local stability of such configurations plays a determining role in the final surface structure after annealing. In this respect attention is also drawn to the influence of bulk dislocations on the nucleation and domain-wall structure of the reconstructed surface.

II. EXPERIMENT

The Au(110) crystal (99.999% purity) was mechanically and then electrochemically polished. The clean surface was prepared by prolonged cycles of low-energy Ne ion bombardment and annealing at a temperature of 750 K. *In situ* x-ray photoemission spectroscopy (XPS) and LEED were used to control surface contamination and surface ordering, respectively. Initially, elongation of the (1×2) LEED spots was observed to be consistent with one-dimensional disorder. This effect was diminished with sputtering/annealing cycles until a sharp (1×2) LEED structure was observed. The STM was connected to a conventional combined XPS-LEED system and samples were transferred to the microscope under UHV ($p\leq10^{-8}$ Pa).

The STM tips were electrochemically etched from polycrystalline W wire and mounted on a tip-transfer holder where they were heated to ~1300 K in UHV and later sharpened using Ne ion bombardment prior to being mounted in the STM just before imaging the surface. The STM was previously calibrated for sensitivity and orthogonality in the lateral scan directions using the Si(111)$-(7\times7)$ reconstruction and in the vertical direction using a stepped Cu(111) surface exhibiting a variety of steps of monatomic up to quadroatomic size. The data were acquired using an IBM PC-AT system described elsewhere.[25] Briefly, all data sets were recorded using 16-bit analog-digital converters and the scanning was achieved using 16-bit digital-analog converters. Two types of STM image were recorded in this study. First, conventional STM topographs were recorded at constant tunnel voltage V_t and tunnel current i_t. The actual values are indicated in the figure captions and they were selected to give the best image quality. They depended on the tunnel-tip condition and do not usually reflect changes in surface condition. Second, we found it convenient to also record differential STM images[26] simultaneously in certain cases (particularly on highly stepped surfaces). Here the tip was modulated in the x direction by ~0.2 Å at a frequency of ~7 kHz, well above the scanner resonance frequency ($f_0=2$ kHz) and the response dI/dx recorded using phase-sensitive techniques. A discussion of this procedure is published elsewhere.[27] Unless stated, no post-processing was done on the images and various visualization routines were used to render the STM topographs as gray-scale topview images or in other more sophisticated ways when appropriate.

III. RESULTS AND DISCUSSION

A. (1×2) domains

Extensive sputter-anneal cycles are required to produce a sharp LEED pattern. Our STM measurements indicate that (1×2) domains of dimensions of several thousand Å can be achieved with a minimum of defects. Figure 1 shows an example of a 670×670-Å^2 area of the surface exhibiting an almost perfect (1×2) phase in which atomic rows separated by 8.16 Å are clearly resolved, the corrugation amplitude being 0.8 Å at tip voltage $V_t=0.37$ V and set current $i_t=250$ pA. No atomic resolution was observed along the rows. Just at the bottom of Fig. 1, a single atomic step (1.4 Å high, marked *S*) is observed running along $[1\bar{1}0]$ corresponding to a (111) microfacet. In general, the steps show long-range ordering in $[1\bar{1}0]$ whereas kinks in [001] exposing (100) facets are rarely observed to be longer than several atomic distances. Figure 2(a) shows a 3000×3000-Å^2 area of the surface recorded during a different experimental run. Owing to a limitation on the number of data points, governed by the computer memory size, the (1×2) corrugation cannot be recorded. However, we confirmed its existence during the *total* scan by monitoring the z signal on a storage oscilloscope and by recording smaller areas in the field of view, one of which is shown in Fig. 2(b). Our principle

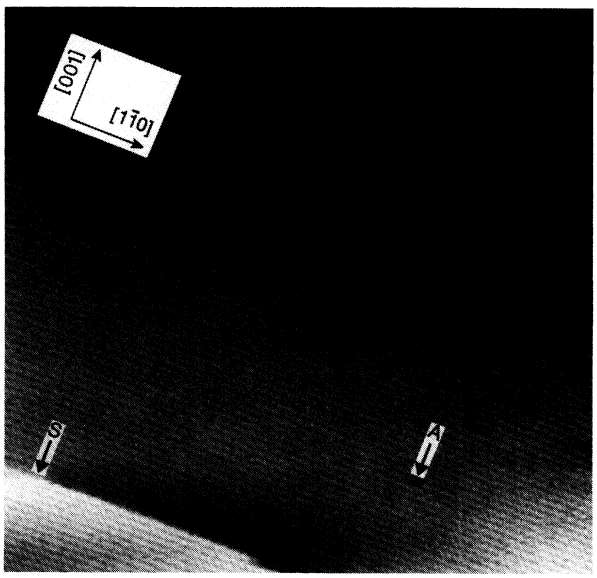

FIG. 1. Gray-scale image of STM topograph from the Au(110) surface exhibiting (1×2) reconstruction. Notice atomic step in bottom left of picture. Area $=670\times670$ Å^2. $V_t=0.37$ V, $i_t=350$ pA.

observation is that the (1×2) domains have large spatial extensions and are separated by staircases of step structures forming bands in [1$\bar{1}$0]. In general, step structures are to be expected on the crystal due to local crystal misorientations. These STM observations of large area scans go beyond previous LEED analyses[4,18,19] and show that the necessary step structures tend to condense into bands rather than being uniformly distributed over the surface in the form of periodic terraces separated by monatomic steps. However, the steps in the bands themselves are distinctly monatomic separated by small (1×2) cells except, as discussed later, in the region of dislocations where fractional step heights are observed. The former behavior is in contrast with observations of fcc (111) surfaces such as on Cu and Au (Ref. 28) where double, triple, and quadruple atomic steps are observed. No evidence was found in our investigation for condensation of steps into facets of greater than monatomic height, suggesting repulsion between steps which nevertheless exhibit bunching. This observation may indicate a longer-range attractive interaction. Another possible mechanism for the apparent condensation may be pinning of steps which migrate over the surface during annealing.[29]

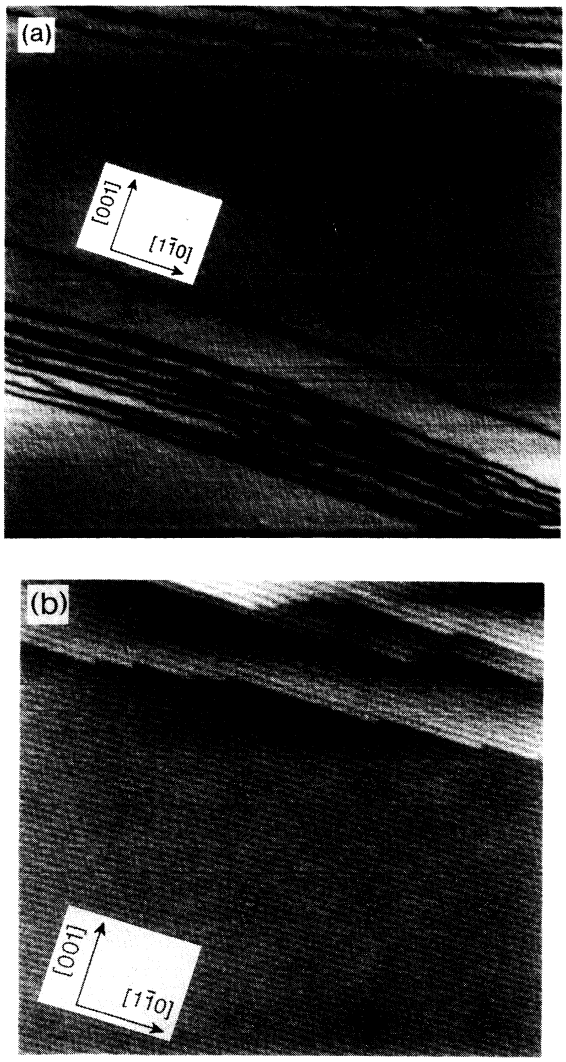

FIG. 2. (a) Pseudoilluminated 3D image of STM topography from the Au(110) surface recorded on a different run from data shown in Fig. 1. Bands of atomic steps are observed in upper- and lower-middle parts of image. Area denotes =3000×3000 Å^2. V_t=0.78 V, i_t=350 pA. (b) Gray-scale image of an STM topograph from Au(110) recorded in the upper left corner region of (a) showing the (1×2) reconstruction and a cluster of atomic steps at the top of the figure. Area .=650×650 Å^2. V_t=0.08 V, i_t=350 pA.

The differences between the virtues of STM and diffraction techniques become very evident from inspection of the (1×2) domain dimensions in Fig. 2(a). Here the STM images show that domain dimensions clearly exceed the typical coherence lengths of LEED or atom-scattering experiments,[30] STM being particularly sensitive to the step structure. If STM topographs were analyzed from small scan areas of the surface one might come to the conclusion that the surface is well ordered or disordered depending on the particular area where the tip happened to be positioned. Hence, any realistic discussion of the nature of the Au(110) surface requires an overview of extended surface areas (several thousand Å in size) from many experimental runs to exclude artifacts or anomalous local surface properties. In the following section we shall direct our discussion on the nature of the disordered areas. For investigation of the (1×2) domains, diffraction methods are better suited since they represent an average over mm-sized areas of the crystal. The utility of STM here lies in elucidating the local shape and nature of antiphase boundary or domain wall structures and their temporal evolution.

B. Antiphase domain walls

There are two equally probable ways to create the (1×2) reconstruction which differ only in terms of a translation vector of one lattice constant in [001]. Nucleation of both types of antiphases may then result in formation of domain walls. The boundary between such domains can be realized in two ways as considered by Moritz, Jagodzinski, and Wolf.[16–19] First, if the domains meet perpendicular to [1$\bar{1}$0] a domain wall structure can be modeled as shown in Fig. 3(a). We shall refer to this as the derailment wall or boundary. Such a phase boundary may be generated by two (1×2) antiphases meeting on a flat surface. The result is a phase shift of one-half of a (1×2) unit-cell distance in [001] between the superstructures. This boundary, as will be shown later, is pinned and requires a concerted translation of the atomic rows of one phase in [001] to coalesce into a monophase.

Alternatively if domains run into each other parallel to [1$\bar{1}$0], the resulting domain wall will consist of either a local (1×1) or (1×3) phase. The presence of a (1×1) region is generally considered energetically unfavorable and we have observed it only within (331) microfacets at terrace edges on clean Au(110). By adding an atomic layer [see Fig. 3(b)] the (1×1) or (1×3) phase is transformed into a step. Here a phase shift of one-quarter and three-quarters of the (1×2) unit-cell distance occurs in [001], respectively. Steps in [1$\bar{1}$0], observed previously with

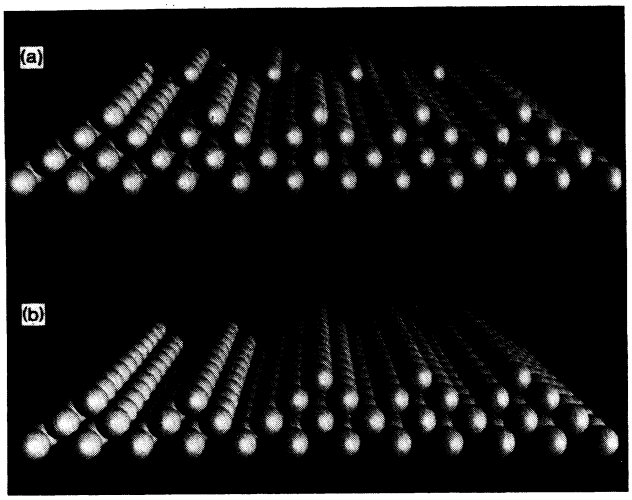

FIG. 3. Models of antiphase boundaries for a Au(110)(1×2) surface proposed by Wolf, Jagodzinski, and Moritz (Ref. 19). (a) Domain boundary formed vertical to ordered chains with not atomic step by a unit-cell displacement in the origin of the superstructure on a flat surface which we call the "derailment wall." (b) Two ordered domains separated by a (111) step generating a displacement of the origin of the superstructure, which we call a "step" wall.

STM,[9] appear to play a dominant role in surface structuring at room temperature. Step boundaries usually expose a (111) microfacet. Theoretically, glue-model calculations indicate that this boundary is only slightly less stable than the (1×2) monophase.[1] To date, the derailment boundary has not been observed on Au(110)(1×2), although its existence has been postulated. Figures 4(a) and 4(b) show detailed STM images of both types of antiphase boundary which were taken from larger-scale topographs. In Fig. 4(a) the (1×2) rows in both phases are well resolved. However, at the domain wall there is an apparent loss of resolution which results in a diffuse boundary region, which is almost perpendicular to the rows and approximately 15 Å wide. Repeated scans of this domain wall (discussed in Sec. III D) show that it is temporally unstable and in a constant state of motion around its pinning points. We interpret this behavior as evidence of significant atomic motion at the derailment boundary, whereas step boundaries are well resolved in [1$\bar{1}$0] indicating their greater stability.

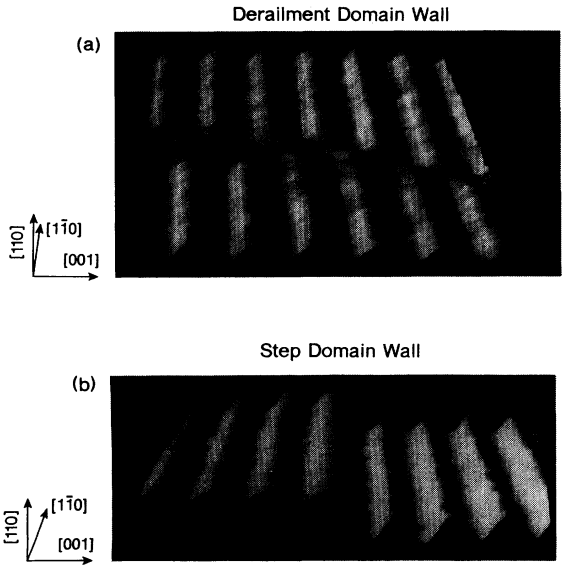

FIG. 4. Pseudoilluminated 3D image of a region of a STM topograph from the Au(110) surface corresponding to the disorder model in Fig. 3. (a) shows the (1×2) two domains displaced by unit cell along the [001] direction displacement forming a derailment domain wall, and (b) shows a domain boundary formed by an additional atomic layer. $V_t = 0.25$ V, $i_t = 150$ pA.

C. Atomic step structures

In the previous section we discussed two ways in which the interface between antiphase (1×2) domains can form energetically favorable boundaries. One of those was the step wall which, at an antiphase boundary, produces a (111) microfacet. If we add an adlayer of atoms in the form of a terrace to a single domain surface (Fig. 5) a (111) microfacet is produced at one side of the terrace and a (331) microfacet or a (1×1) region (inclusion of hatched atom) at the other side of the terrace, both of which are energetically less favorable than (111) steps. If, however, a miniterrace joins two antiphase domains, both sides of the terrace are conveniently terminated by (111) facets. Our infrequent observations of adlayers on monophase terraces indicate that (111) steps preferentially form to energetically stabilize antiphase boundaries in [1$\bar{1}$0]. Figures 6(a) and 6(b) show the STM images of (111) and (331) faceted steps. The slope of the (111) facet (a) is greater than the slope of the (331) facet (b). In addition, the latter shows an additional hump where the (1×1) atomic row is resolved. Another difference between the step structures is that the phase shift between the (1×2) rows on the upper and the lower terrace is larger in (b) by one lattice constant.

We have compared the step profiles shown in Fig. 6 with theoretical calculations of a (111) and a (331) faceted step profile on Au(110)(1×2) made by Tersoff using an atom superposition method.[31,32] We find that in both phase and shape a good agreement between experiment and theory is obtained even for small (1×2) domains. Note that the calculated step profile shown in Fig. 7(a) for a (111) faceted step has a smooth shape even at high resolution, whereas that of a (331) faceted step [Fig. 7(b)] displays an additional bump (see schematic illustration in Fig. 5). This additional feature can be clearly observed in the experimental data [Fig. 6(b)] of a (331) step. It should be noted that the differing phase shifts between the (1×2) rows on the upper and lower terraces provide an additional means of differentiating (331) and (111) steps.

Figure 8 shows a cross section along [001] of a single (1×2) cluster observed on a monophase (1×2) underlayer. Here the cluster sits asymmetrically on the underlayer forming a (331) microfacet on one side and a (111) microfacet on the other. To indicate how well the positions of the maxima in the line profile of the cluster fit with Tersoff's calculation, we have marked the expected

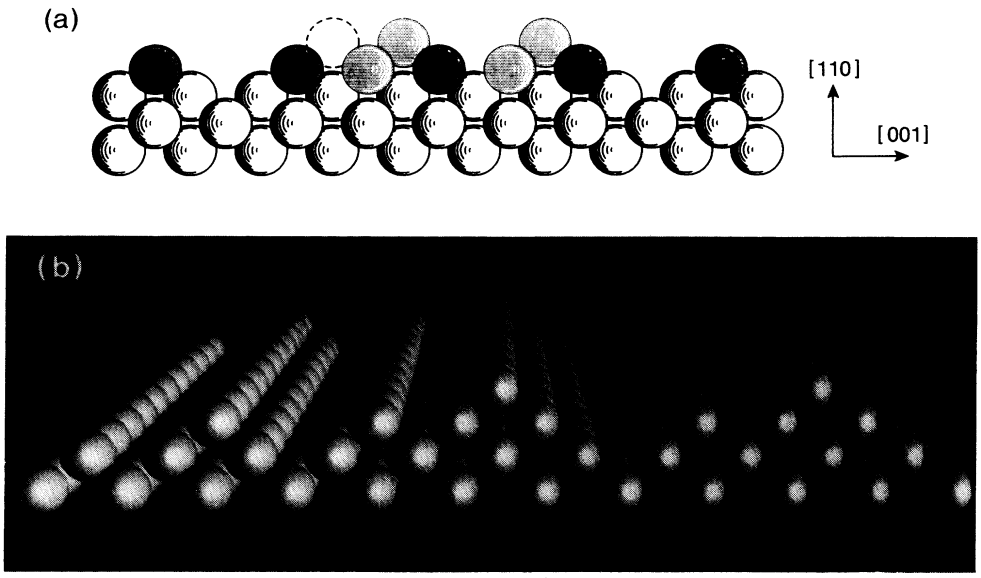

FIG. 5. (a) Schematic illustration of the effect of adding a miniterrace adlayer of Au atoms to a single (1×2) phase. On the left a stable (111) facet may be formed. However, termination of the facet on the right results in a (1×1) row if the hatched atom is present or in a local type (1×3) structure if it is missing. (b) Models of (111) and (331) steps produced by adding additional (1×2) rows to a monophase terrace.

positions of the maxima with tick marks. It can be seen that, within experimental error, even a single (1×2) row fits in with the geometrically expected position based on simple superposition of spherical atomic charge densities.

Preferred distances between steps have been reported for the reconstructed surfaces of Au(100),[33] Au(111),[34] and Si(111).[35] Bartolini, Ercolessi, and Tosatti[36] interpreted these "magic" terrace lengths as surface energy terms which stabilize certain vicinal surfaces. The terms turn out to be minimal whenever the terrace length is able to accommodate an integer number of reconstructed unit cells. In the case of the (1×2) reconstructed Au(110) surface, the predominance of (111) steps compared with (331) steps can be explained in these terms. Roelofs *et al.*[37] have calculated the energetic stability of both

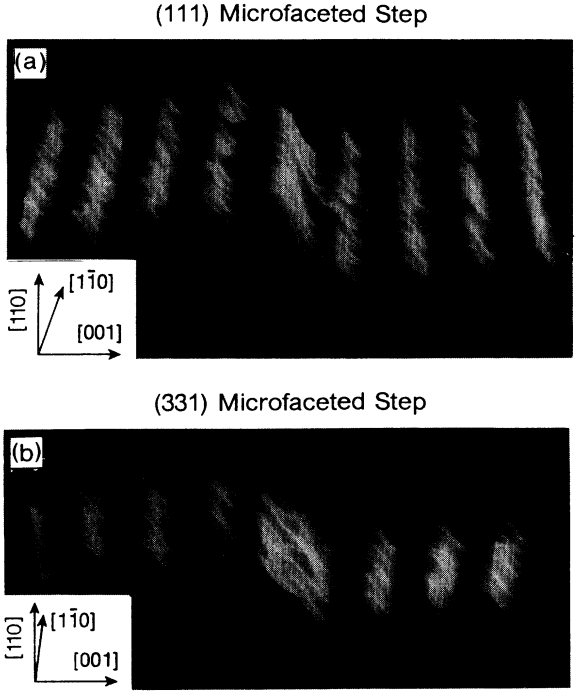

FIG. 6. Pseudoilluminated 3D image of STM images of Au(110)(1×2) showing (a) a step across the [100] direction exposing a (111) microfacet and (b) a step across the [100] direction exposing a (331) microfacet, which is observed only rarely. $V_t = 0.25$ V, $i_t = 150$ pA.

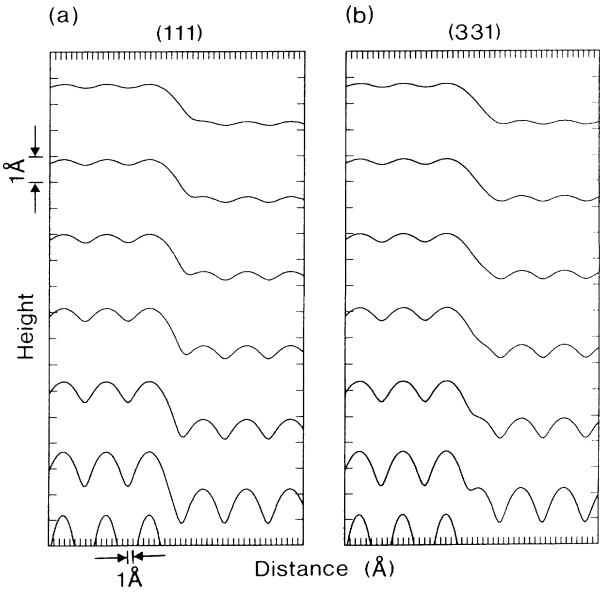

FIG. 7. Image calculated with an atom superposition method (Ref. 32) for (a) a (111) step and (b) a (331) step on Au(110)(2×1). Thus figure shows (1$\bar{1}$0) plane through outermost atoms. Contours reflect different tunneling currents. The tip is represented as a point source.

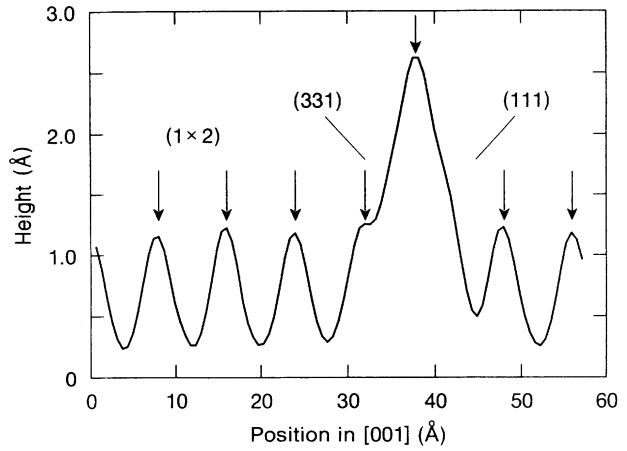

FIG. 8. Line profile across a single additional row of (1×2) on a monophase (1×2) terrace. Asymmetry in structure reflects a (111) microfacet on the right-hand side and a (331) microfacet on the left-hand side of the structure. The arrows indicate position of the maxima determined using a theoretical calculation of (111) and (331) step profiles by Tersoff.

(111) and (331) steps on the (1×2) missing-row phase on Au(110) using an extended embedded atom method. They find that (111) steps are far more probable than (331) steps on energetic grounds in accordance with our observations.

We now turn our attention to steps created perpendicular to the (1×2) rows in the [1$\bar{1}$0] direction. These steps expose a (100) microfacet and are observed to exhibit a markedly different behavior from the step boundaries in [100]. In general our observations show that such step structures exhibit little long-range order and display extreme roughness in contrast to steps running along [1$\bar{1}$0] that are stabilized by the generation of (111) microfacets. Figure 9 shows a stepped area of the surface that illustrates preferential roughness in (100). The (1×2) rows of atoms are clearly resolved and the step structures running across the picture are extended in [1$\bar{1}$0] whereas the exposed (100) facets extend over several rows of the superstructure. Also note that the steps in [1$\bar{1}$0] compared with the steps exposing (111) microfacets apparently show slightly poorer definition. We shall return to this observation in Sec. III E when we discuss the mobility of surface atoms.

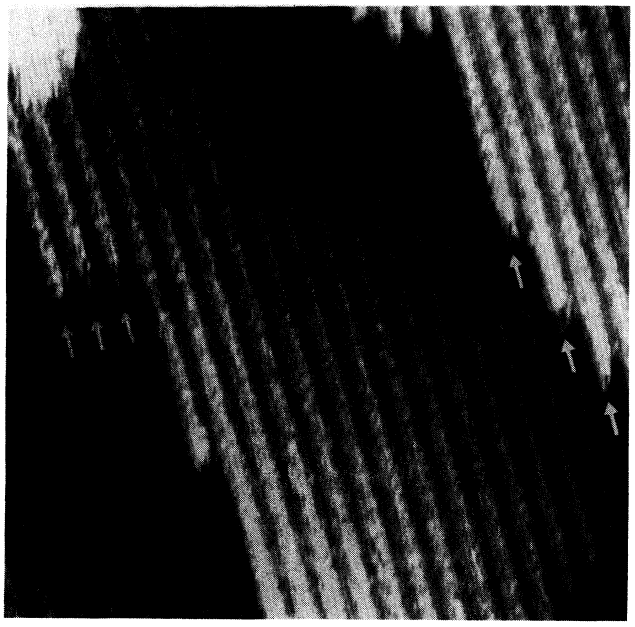

FIG. 9. Detailed gray-scale image of a STM topograph for Au(110) showing a sequence of steps with preferential ordering in the [1$\bar{1}$0] direction and poor ordering in the [001] direction. Note the apparent lack of resolution on particular kinks (arrows). $V_t = 0.56$ V, $i_t = 200$ pA.

D. Observation of bulk dislocations

In Sec. III A we discussed the dimensions of (1×2) domains and the observation of step bunching. Here we shall present evidence of an additional type of domain structure which occurs on the surface and which we have observed to occur in localized patches during quite a number of independent runs. Figure 10 shows a 0.5×0.5-μm^2 area of the surface. The gray-scale image has been post-differentiated to represent dz/dx. We use this technique to improve the visibility of atomic steps (bright bands represent positive slope and dark bands represent negative slope). Due to the limited data point density (1 point/10 Å), the (1×2) phase is not resolved but, as discussed in Sec. III A, all detailed subregions of the image window showed the (1×2) phase to be present in domain dimensions of up to ~1000 Å in [001] and up to ~3500 Å in [1$\bar{1}$0]. Characteristic step bunching with bands directed predominantly along [1$\bar{1}$0] (see B1 and B2) is also observed. The step bands show a "bowing out" as is known for pinned bulk dislocations.[38]

We shall now discuss another characteristic structure

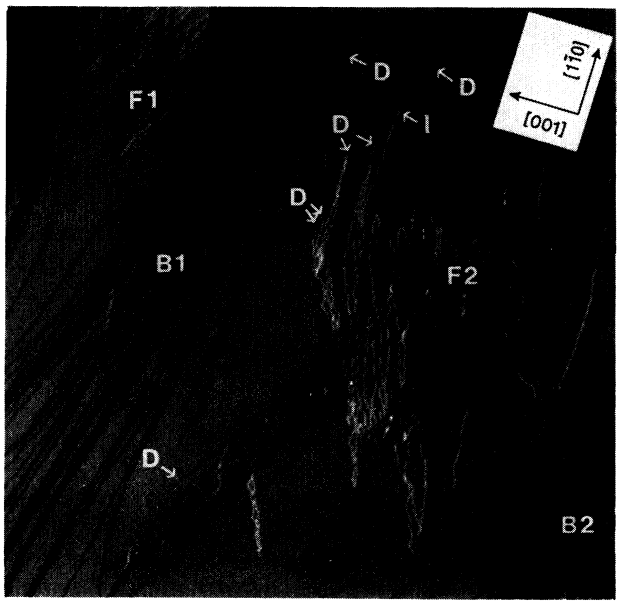

FIG. 10. Gray-scale post-differentiated (dz/dx) image of an STM topograph from a 0.5×0.5-μm^2 area measured at $V_t = 0.25$ V, $i_t = 200$ pA.

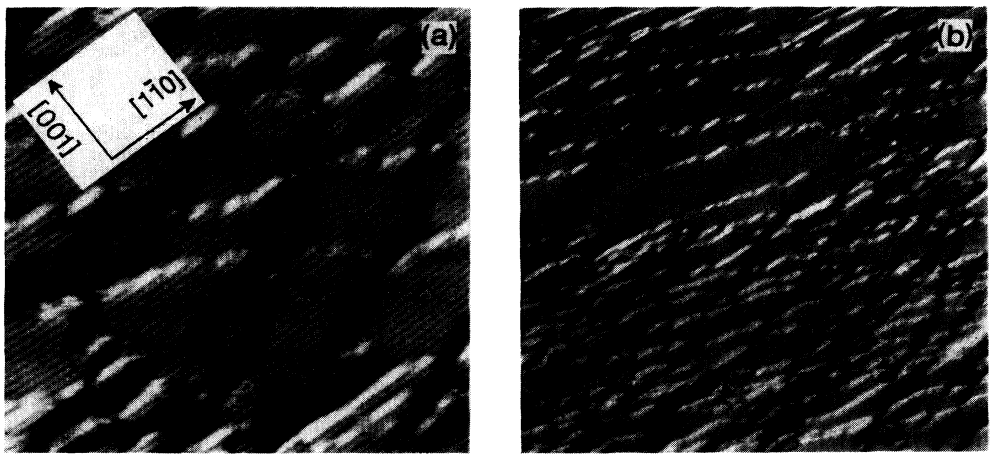

FIG. 11. Gray-scale image of a differential STM topograph from Au(110) showing textured patterns. (a) Area in 550×550 Å^2 and (b) area of 1100×1100 Å^2. Differential topography shows steps as distinct dark or light bands depending on slope sign. $V_t=0.25$ V, $i_t=200$ pA.

observed in regions F1 and F2. Here the step structure can be described in what we term a fish scale pattern where an overall misorientation predominantly in [1$\bar{1}$0] is accommodated by the intersection of two bands of steps, both aligned approximately along a ⟨111⟩ direction. The steps themselves terminate abruptly into flat parts of the surface (see regions indicated D) or even exhibit steps which reverse form positive slope to negative slope (region I). The disappearance of steps into the surface is a signature for the intersection of dislocations with the surface and we shall discuss atomically resolved images of these features below.

Figure 11 shows a detailed region of the fish scale patterns formed by the intersection of bunches of steps with obtuse and acute orientations with respect to [1$\bar{1}$0] observed in an independent experiment. Since the overall effect is a misorientation in [1$\bar{1}$0], one might expect more steps in [1$\bar{1}$0] than in [001]. However, our observations strongly suggest that the shape of the terraces result from stabilization of the (100) microfacets by the (111) microfacets resulting in the fish scale pattern observed. Consequently, although the local misorientation is predominantly in the [1$\bar{1}$0] direction, the resulting step structures exhibit considerable (111) faceting.

Figure 12 shows another atomically resolved image of a fish scale region. We note that the pattern is associated with a large number of antiphase boundaries on the surface, i.e., between each terrace on the same atomic plane one can identify a shift of the superstructure by $\frac{1}{2}$ of a unit cell. The step edges are all of the (111) type with kinks in [001]. Given the phase shift between adjacent terraces, (111) steps cause an additional $\pm\frac{1}{4}$ superstructure unit cell phase shift depending on whether the step direction is upward or downward. They have the effect of regenerating an antiphase boundary of $\frac{1}{2}$-superstructure unit cell between terraces associated with a given side of the triangular step structure. We would like to suggest that the presence of bulk dislocations at the surface certainly appears to play an important role in the nucleation of the (1×2) phases as evidenced by the large number of antiphase domain walls observed in the region of the dislocation. This point will be elaborated on when we show evidence for additional phase shifts between domains resulting from partial dislocations.

To recap, step structures terminate in a manner typical of the presence of bulk dislocations intersecting the surface. Terminated step structures are associated with fish scale patterns suggesting that the nucleation of the (1×2) superstructure, in particular phase-matching conditions, are affected by the presence of these bulk dislocations. Local distortions of the surface atomic positions introduced by the above phenomena are now addressed.

Figure 13 shows an atomically resolved image near the core structure (C) of a dislocation where it emerges at the

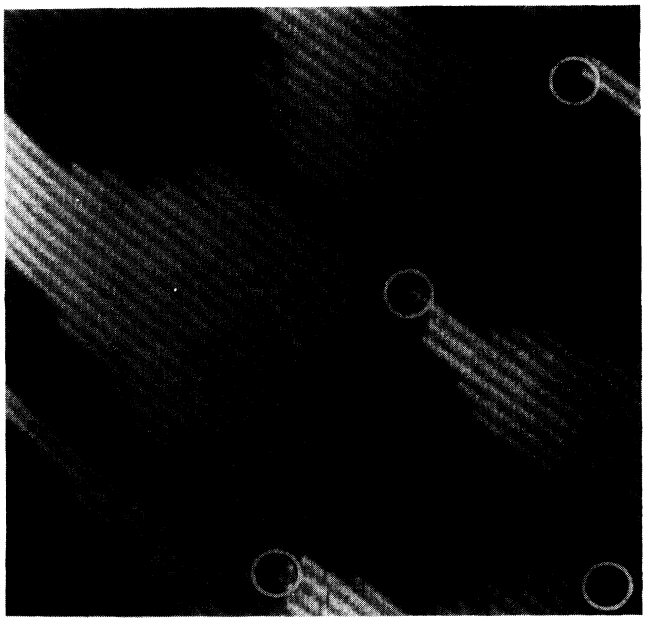

FIG. 12. Detailed gray-scale image of a STM topograph from Au(110) showing steps forming a textured pattern. The (111) steps delineate antiphase domains.

surface. Two forms of representation have been used to illustrate the essential observations discussed below. Two clusters (I1 and I2) consisting of an additional single row (height denotes 1.4 Å) are visible. What is particularly relevant is the presence of two steps, S1 and S2, observed in the image which have a height of only $\frac{1}{2}$ of a normal step in the region of C and which gradually increase their height as the distance from the core increases. In addition the monophase (1×2) region of the surface is heavily distorted and can be described in terms of a helicordal structure centered at (C). The formation of a shift in the lattice by $\frac{1}{2}[110]$ is typical of the slip of closely packed $\{111\}$ planes and can be invoked to explain the observation of the step height near C. The unit dislocation with a Burgers vector in [110] is achieved by two vectors $\frac{1}{2}[110] \rightarrow \frac{1}{6}[211] + \frac{1}{6}[12\bar{1}]$. This unit dislocation is typical of fcc metals. Recently a similar stacking fault was atomically resolved on Cu(111) using STM where the dislocation emerges in the form of steps of $\frac{1}{3}$ or $\frac{2}{3}$ the height normally observed on the (111) surface. The resulting stacking fault generates quite a large region of distortion in the region of the partials.[39]

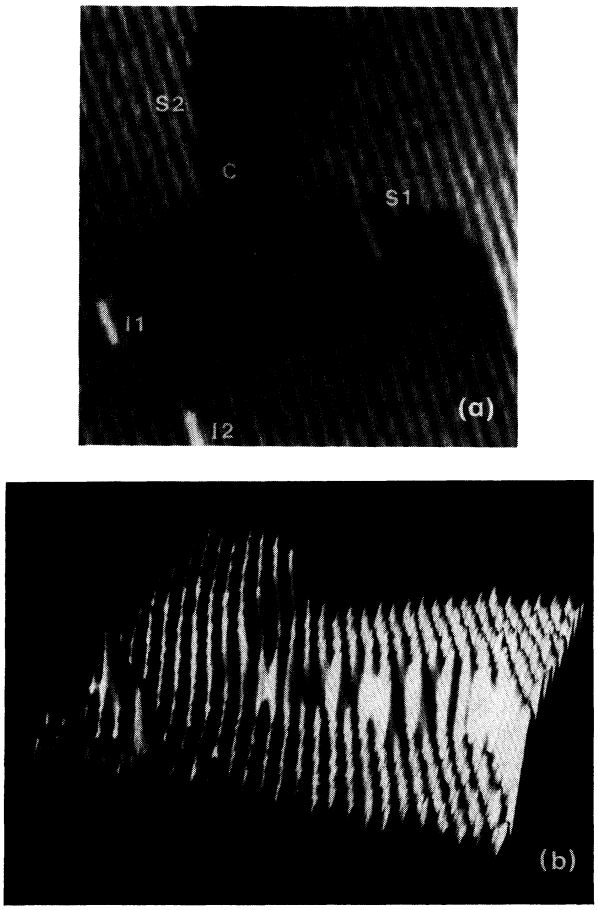

FIG. 13. (a) Gray-scale image of a STM topograph of a dislocation emerging from the surface (see text for explanation of marker). Area $=240\times240$ Å^2, $V_t=0.37$ V, $i_t=200$ pA. (b) Pseudoilluminated 3D representation of (a). Note that filtering was applied in (b) to reduce the corrugation amplitude enabling the dislocation to be better visualized.

Despite the distortion introduced by the stacking fault, it is evident from Fig. 13(b) that the (1×2) reconstruction persists over the entire region around point C. An intriguing aspect of the $\frac{1}{2}$ atomic step introduced by the dislocation compared to the monatomic step that develops at the periphery of Fig. 13, in addition to the distortion of the superstructure in [110], is that different phase shifts occur due to the stacking faults. Recalling that a (111) monatomic step introduces a $\frac{1}{4}$ superstructure cell shift in [001] we calculate that the respective shift for the $\frac{1}{2}$ step height is $\frac{5}{12}$. The (1×2) rows, therefore, accommodate a 16% distortion of the superstructure in [001] with no distortion calculated for the atomic positions in $[1\bar{1}0]$. The above discussion implies that the minimization of the surface free energy by formation of a (1×2) reconstruction dominates over the presence of a highly strained bulk lattice and that distortions can be accommodated by the atomic rows.

Additional defect structures and effects induced by contamination and adsorption are now discussed. The simplest defect for a surface is missing atoms or adatoms. Figure 14 shows a block of four Au atoms missing from an atomic row in a (1×2) reconstructed area (A). This kind of defect is rarely observed[40] (less than once per 10^5 surface atoms) on the flat areas as well as on more stepped structures. Here we include the possibility that there are foreign atoms embedded in the surface whose local density of states in the tunnel voltage region is negligible, however, there are certainly no gold atoms present in the defect region.

Individual Au adatoms, although probably present on the surface, are extremely mobile and we have found no evidence of them in the topographs. However, during our measurements the tip was occasionally sharpened by applying a short pulse ($\sim$10 ms at 5 V). This leads to

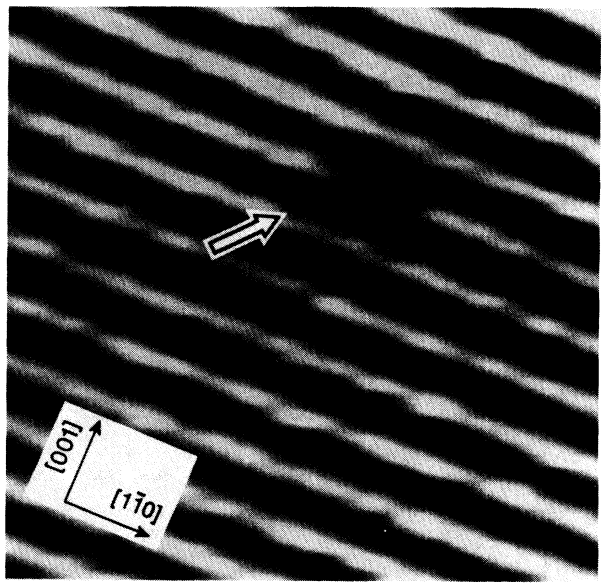

FIG. 14. Gray-scale image of a STM topograph of four missing atoms in a row of the (1×2) reconstruction. $V_t=0.25$ V, $i_t=200$ pA.

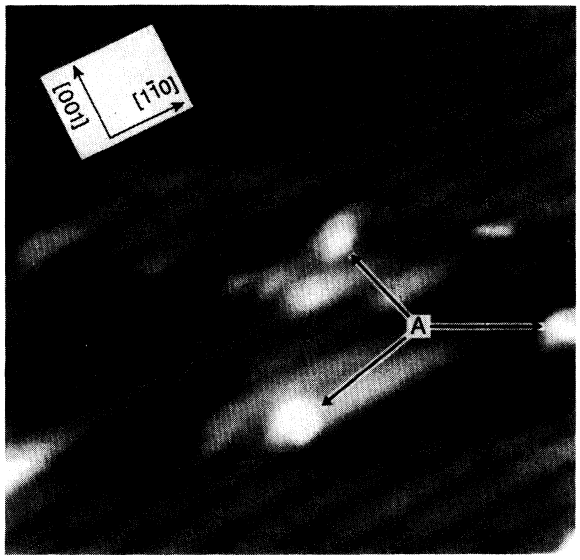

FIG. 15. Gray-scale image of a STM topograph of Au(110) showing three small structures deposited by pulsing the tip at +5 V for 10 ms. The structures are ~3 Å in height and their shape was independent of tip polarity within the range $|V_t| < 1$ V.

field desorption of tip adatoms. Figure 15 shows three clusters or atoms deposited from the tip after desorption; they are approximately 3 Å in height and their structure was found not to depend on tip polarity. We ascribe these features to foreign atoms.

We next discuss the effects of contamination of the reconstruction. Gold surfaces are known to be extremely stable to contamination. Even more than 3 days after preparation the (1×2) reconstruction persists in bad UHV conditions. Figures 16(a) and 16(b) show an example of STM image recorded after 80 h exposure to UHV at $p \approx 5 \times 10^{-10}$ mbar. In comparison with the previous figures, the overall topography displays significant differences. On the left-hand side of Fig. 16 we observe an apparently amorphous area consisting of a rough [1$\bar{1}$0] texture which slowly transforms into a more ordered sequence of (1×2) rows of finite extension interspersed with steps in the [001] direction, resulting in what was previously described as a local (1×3) phase.[9] We discount that the observed structural changes are due to an abrupt change in tip condition since on the top right of the picture a similar amorphous patch is also evident, and also since there is no abrupt spatial change in the order-disorder transition region. In the *ordered* region we typically observe two to four rows of (1×2) reconstruction separated by steps. The structure along these rows appears to be somewhat noisy. These results indicate that contamination destabilizes the long-range order and generates amorphous patches. Such a stabilization of the (1×3) phase has been reported for submonolayer Cs adsorption[41] and STM results also indicate formation of a (1×3) phase.[20] We ascribe the change in structure to CO adsorption which represents the major source of contamination in our UHV system.

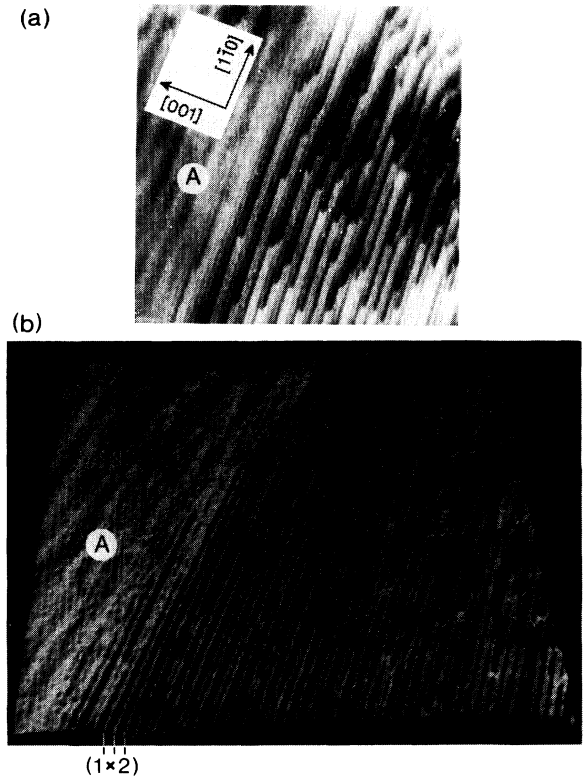

FIG. 16. (a) Gray-scale image of a STM topograph from contaminated Au(110). (b) Pseudoilluminated 3D representation of the same topograph. Area = 500×500 Å^2, recorded ~80 h after preparation and left in a UHV at $p \sim 4 \times 10^{-10}$ mbar. Topographs of the fresh film were similar to previous figures.

E. Surface mobility

Binnig *et al.*[9] suggested that mass transport via kinks might occur in rows along the [1$\bar{1}$0] direction. Rearrangements of atomic columns on gold surfaces including (110) were found to be highly mobile as shown by time-lapsed high-resolution TEM.[42] In our study we have observed that even at room temperature, considerable differences can be detected between consecutively recorded pictures.

To investigate the temporal changes of the surface in more detail, we observed the evolution of a variety of regions of the surface using time-lapse sequences of images. Figures 17(a)–17(d) show four images selected from a series of topographs of a 400×400-Å^2 area of the surface repeated every 2 h. In Fig. 17(a) we note that the surface comprises a series of step structures containing mainly (1×2) atomic rows and that in the center of the picture a miniterrace of dimension ~50×100 Å^2 is clearly resolved. The next obvious observation is that between Figs. 17(a) and 17(d), a variety of structural changes have occurred in the step structure and miniterrace shape although a semblance of similarity still exists after a period of ~6 h. At the tunneling parameters used in our experiment, we expect the influence of the tip on surface mobility to be small. This assumption is supported by the observation that even after several scans over a particular region no tip-induced effects could be recognized when

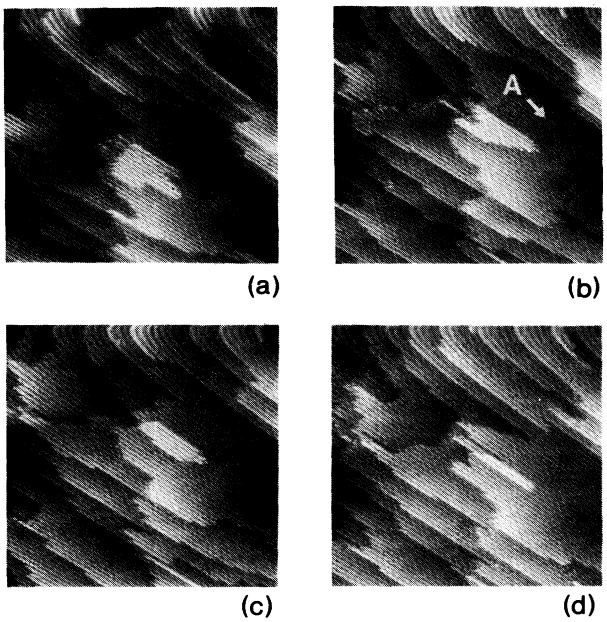

FIG. 17. (a)–(d) Gray-scale images of a 400×400-Å^2 STM topograph of Au(110) recorded at two-hour time intervals. The apparent bending of atomic rows at the tops of the pictures is due to creep of the piezoelectric scanners.

the scan range was enlarged.

We performed a detailed analysis of the series of pictures and we now use the basic building blocks described in Secs. III A–III C to analyze the more essential details of disorder in this picture. First, in region A of Fig. 17(a) we observe a derailment antiphase domain wall [previously shown in Fig. 4(a)] which collapses during a time-lapse sequence of images. Selected images of the temporal disintegration of the domain wall are shown in Figs. 18(a)–18(c). As discussed previously, this domain boundary is rather ill-defined due to surface mobility. It is observed to begin collapsing in Fig. 18(b) where six atomic rows have been displaced by a [100] unit cell to register in phase with the larger domain. By Fig. 18(c) this process has developed further and only three (1×2) rows are out of phase. The process appears to require considerable cross-channel motion. Although our STM observations suggest that the process is abrupt with respect to the measurement time, i.e., a progressive cross-channel transport of single atoms is not observed on the time scale of the sequence of images, further studies at low temperature are required to elucidate the transport process. The movement of atoms across or over rows has been investigated by Wrigley and Ehrlich.[43] They have demonstrated that W atoms on Ir(110) surfaces move preferentially through $[1\bar{1}0]$ rows.[44]

Local areas of (1×2) phase can resemble monatomic clusters or miniterraces. Figure 19 shows a sequence of STM images of a miniterrace structure which is initially $\sim50\times100$ Å^2 in size. With time-lapse images we can directly visualize the gradual evolution of this structure. From image to image a variety of changes in the miniterrace occurs, although the (1×2) phase remains distinctly of monatomic height and has a perfect internal (1×2) ordering. However, there is a general trend in the sequence (a)–(m) for atoms to leave the structure, resulting in a diminuation in the number of atomic rows in $[1\bar{1}0]$ but not in their average length. Even in Fig. 19(m) when only two atomic rows remain, the miniterrace retains its identity.

These observations are in accordance with our previous discussion relating to the relative stability of Au adatoms at various surface sites. Individual atoms are not observed on the surface. Evidence of nucleation and migration along $[1\bar{1}0]$ towards (100) microfaceted kinks results in long rows of atoms exposing dominantly (111) microfacets. The interaction of the missing rows with each other appears, from our observation, to be weaker based on the anisotropy of the dissolution of the miniterrace, however, some form of stabilization does, nevertheless, appear to exist.

Usually steps are observed to extend over several hundred Å in $[1\bar{1}0]$, whereas they expose one or two atom

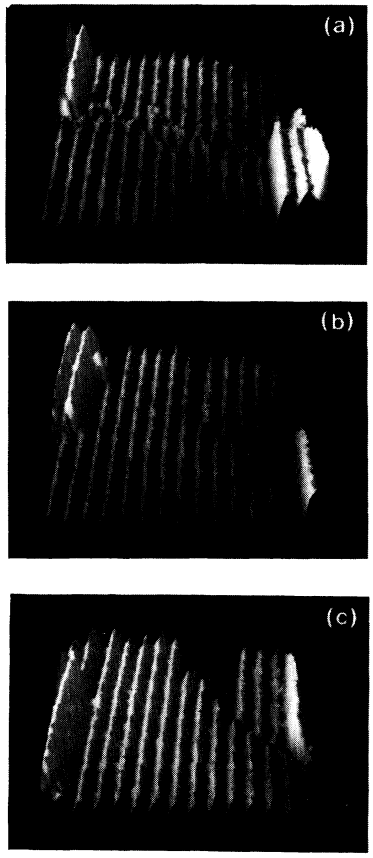

FIG. 18. Pseudoilluminated images of STM topographs of a 120×170-Å^2 area of Au(110) selected from a series recorded at time intervals of 30 min, with $V_t=0.25$ V and $i_t=150$ pA. The surface shows (1×2) reconstruction. Horizontally, a domain boundary separates two (1×2) domains, which are displaced by one lattice constant in the [001] direction. The domain boundary initially extends over eleven (1×2) atomic rows and collapses down to three out of phase rows in the later stages of the measurement. On the time scale of measurement, rows apparently jump instantaneously in a concerted fashion.

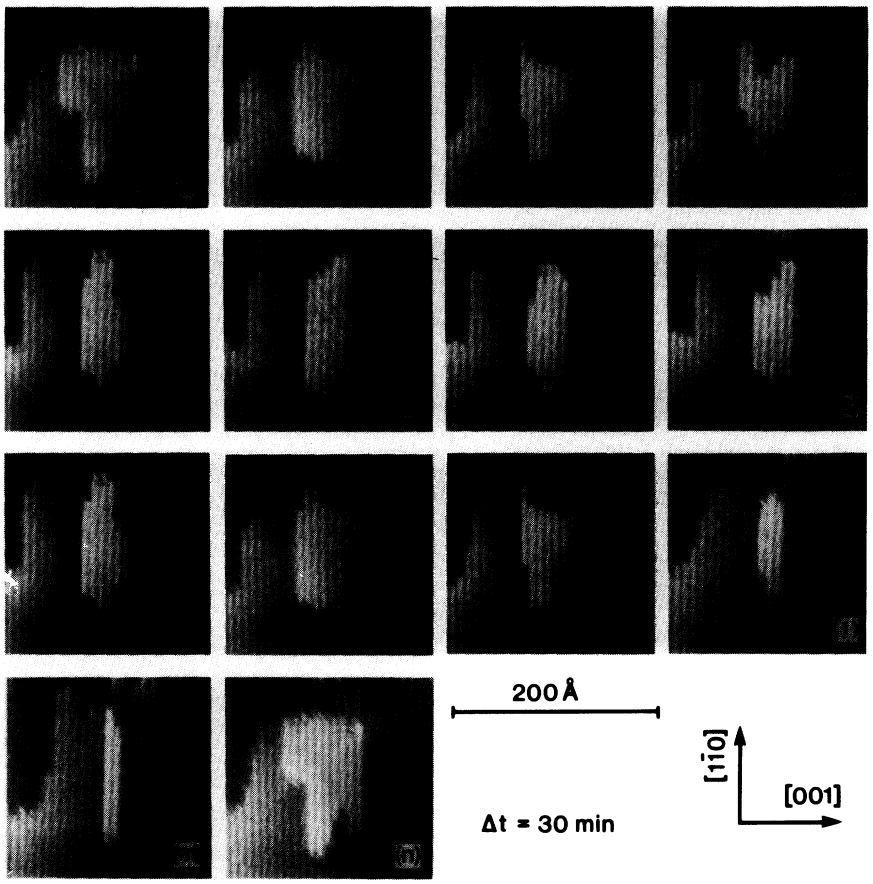

FIG. 19. Sequence of gray-scale images of STM topographs which display structural changes occurring at a (1×2) reconstructed miniterrace. The time interval between each picture is 30 min. Part (n) is a repetition of (e). Over the total measurement time of 6 h the miniterrace gradually dissolves from (d) initially 12 rows to (m) 3 rows.

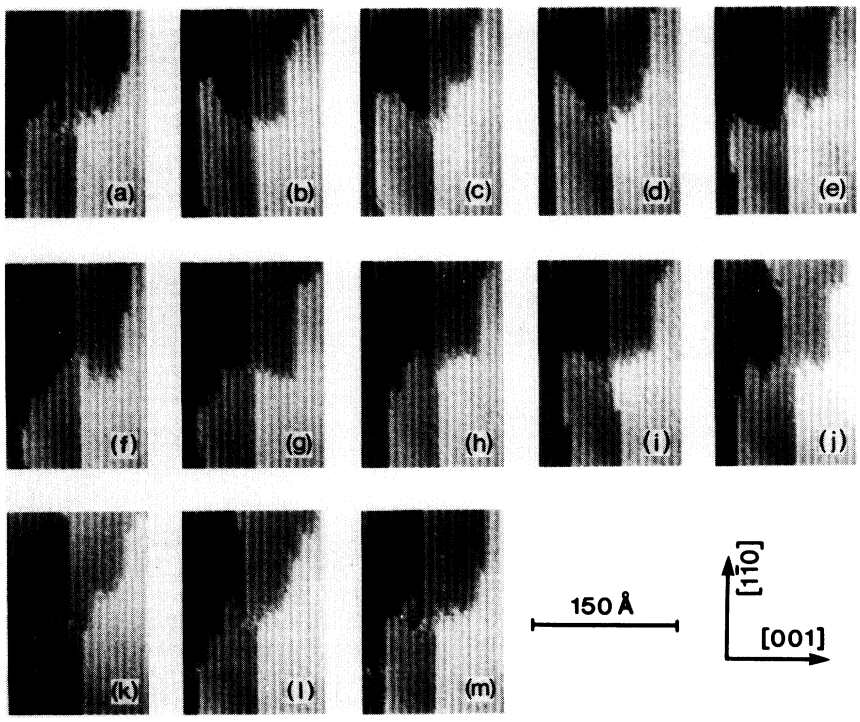

FIG. 20. Time series of gray-scale images of STM topographs recorded every 30 min showing the development of a (1×2) reconstructed area which is divided into three terraces by monatomic steps. The middle and top terrace expose unusually wide steps along the unfavorable [001] direction. These steps meet in all the pictures creating a convenient reference point.

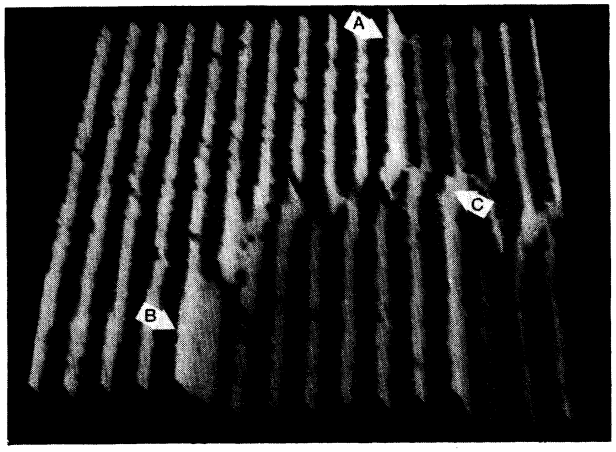

FIG. 21. Detailed pseudoilluminated 3D representation of Fig. 20(a). The atomic rows along the [1$\bar{1}$0] azimuth are visible on three terraces. The middle terrace consists of two domains separated by a derailment boundary marked C. The displacement by one lattice constant of the underlying gold crystal between these domains forces the topmost terrace to form a (111) microfacet step in the upper part of the surface (A) and a (331) microfacet step in the lower part (B).

kinks perpendicular to the close-packed rows. Figure 20 shows the temporal evolution of a stepped surface region, taken at 30-min intervals. The area is split into three terraces by monatomic steps. In contrast to the behavior mentioned above, the middle terrace shows a step towards the lowest terrace along [001], which is up to seven rows wide. The highest terrace, in turn, exposes a similar boundary towards the middle region. A remarkable feature in this sequence of images is that both steps appear to be linked. They meet in the center of any of the pictures. In fact, this point was used as a reference when extracting these pictures from larger-area scans. Due to the high mobility observed on the Au(110) surface it is usually impossible to locate any fixed point in a series of topographs. Here, however, it is possible to judge the relative positions of steps. The reason for the extraordinary stability becomes obvious in Figs. 20(a), 20(d), and 20(m). The middle terrace is separated into two domains by a phase boundary exactly where the [001]-directed steps meet. This is displayed in greater detail in Fig. 21, which is a pseudo-3D representation of Fig. 20(a). The middle terrace is divided into two antiphase areas by a derailment boundary marked "C" in Fig. 21, resulting in a shift of one lattice constant of the underlying gold lattice in [001]. Since the topmost terrace forms a single (1×2) domain, steps (A) and (B) must have a different atomic geometry. By comparison with the basic step structures discussed in Sec. III C, we can unambiguously identify them as (111) and (331) structures, respectively.

Locally, antiphase domain boundaries can stabilize unstable structures. As in the case described above, they can be viewed as local defects where the kinetics of the nucleation of the reconstruction are significantly modified.

F. Anomalous corrugation

A corrugation along densely packed atomic rows has not usually been observed. Rarely, however, was it possible to obtain images like those shown in Fig. 22. The measurement was made at the rather usual tunneling parameters of $i_t = 1$ nA and $V_t = -0.8$ V. Rows along [1$\bar{1}$0] exhibit a corrugation of 0.3 Å with a periodicity of 2.9 Å corresponding to the nearest-neighbor distance of gold. The corrugation across rows amounted to an anomalously large value of 1.4 Å, clearly indicating electronic effects to be important. Atomic rows appear strongly asymmetric. This might hint at an asymmetric tip able to atomically resolve (111) microfacets on one side of the rows.[45]

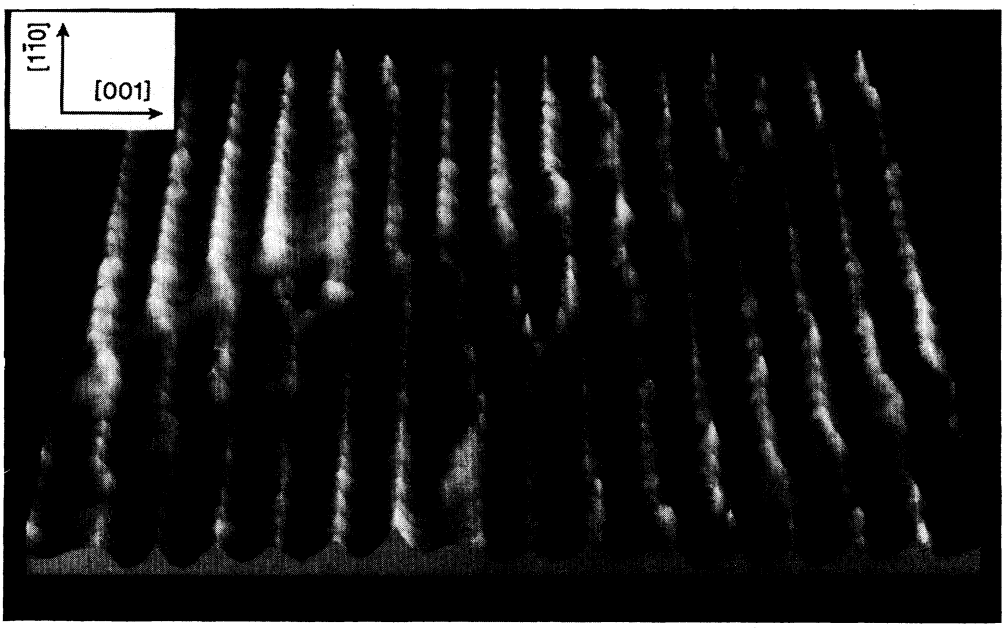

FIG. 22. Pseudoilluminated 3D representation of a topograph from an area (120×90 Å^2) recorded at $i_t = 1$ nA and $V_t = -0.8$ V. Rows along [1$\bar{1}$0] exhibit a corrugation of 0.3 Å with a periodicity of 2.9 Å corresponding to the nearest-neighbor distance of gold.

IV. CONCLUSIONS

The measurements presented above show that (1×2) reconstructed Au(110) surfaces can be prepared to a reasonable degree of perfection, resulting in defect-free areas larger than typical coherence lengths of scattering experiments. However, during the initial phase of crystal preparation we did observe highly stepped surfaces consisting of small ($\approx$5000 Å^2) (1×2) facets. With successive sputter-anneal cycles, areas extended some 500 000 Å^2, and were separated by monatomic steps which condensed into characteristic bands.

Our observations indicate that only monatomic steps are dominant, and that they expose either a (111) or, to a much lesser extent, (331) microfacet since these have the lowest surface free energy. (331) facets are necessary to bring (1×2) islands into registry with an underlying (1×2) monophase. In [1$\bar{1}$0], steps extend over several tens of Å. Kinks, which cause (100) facets to occur, are much shorter, extending typically over a few atomic rows.

Whereas perfectly ordered areas of the surface appear to be basically static, the stepped regions show temporal changes which provide a useful insight into the kinetics of the surface reconstruction. On the time scale of our experiment we observe movements of kinks over several Å/min and hopping of complete atomic rows, as evident in the region of the antiphase boundaries. These fast changes in the surface geometry may be responsible for the rareness of derailment phase boundaries. Initially, atoms may register into two equally probable sublattices. However, since the atomic movement along step and kink sites appears to be fast, any step will rapidly spread one-dimensionally over large distances in [1$\bar{1}$0]. Phase boundaries parallel to the atomic rows are easily avoided by monatomic steps. Thus the probability of finding the instance of a derailment domain wall is relatively low compared with that of a step domain wall.

Finally our results show that STM can be used to investigate finer details of the growth of the surface reconstruction. They show that the temporal evolution of the surface should be considered in systems where sufficient surface mobility occurs and that kinetics strongly influence surface as well as purely thermodynamic considerations. The role of bulk dislocations in the perfection of surface domain size has been addressed. Bulk dislocations do play an important role in step structure and spatial anisotropy of step density.

ACKNOWLEDGMENTS

We wish to thank the following people who, by freely sharing their knowledge, helped us with our study: Alexis Baratoff, Jürgen Behm, Hans-Werner Fink, Franco Jona, Michele Parrinello, Bruno Reihl, Karl-Heinz Rieder, Heini Rohrer, Jürgen Sass, John Spence, and Erio Tosatti. In particular, Jerry Tersoff is gratefully acknowledged for performing theoretical calculations of the step profiles and Erich Stoll for constructing computer models of the reconstruction.

---

*Electronic address: GIM@ZURLVM1 (Bitnet).

[1]F. Ercolessi, M. Parrinello, and E. Tosatti, Philos. Mag. A **58**, 213 (1988).

[2]W. Moritz and D. Wolf, Surf. Sci. **88**, L29 (1979).

[3]J. R. Noonan and H. L. Davis, J. Vac. Sci. Technol. **16**, 587 (1979).

[4]W. Moritz and D. Wolf, Surf. Sci. **163**, L655 (1985).

[5]K. H. Rieder, T. Engel, and N. Garcia, in *Proceedings of the Fourth International Conference on Solid Surfaces and the Third European Conference on Surface Science, Cannes, France, 1980,* edited by D. A. Degras and M. Costa [Vide Couches Minces **1**, 861 (1980)].

[6]M. Manninen, J. K. Norskov, and C. Umrigar, Surf. Sci. **119**, L393 (1982).

[7]T. Engel and J. H. Weave, Surf. Sci. **164**, 403 (1985).

[8]L. D. Marks, Phys. Rev. Lett. **51**, 1000 (1983).

[9]G. Binnig, H. Rohrer, Ch. Gerber, and E. Weibel, Surf. Sci. **131**, L379 (1983).

[10]R. J. Behm, *Scanning Tunneling Microscopy and Related Methods,* Vol. 184 of *NATO Advanced Study Institute, Series E: Applied Sciences* (Kluwer, Dordrecht, 1990), p. 173.

[11]I. K. Robinson, Phys. Rev. Lett. **50**, 1145 (1983).

[12]J. Möller, H. Niehus, and W. Heiland, Surf. Sci. **166**, L111 (1986).

[13]M. Copel and T. Gustafsson, Phys. Rev. Lett. **57**, 723 (1986).

[14]H. J. Broksch and K. H. Bennemann, Surf. Sci. **161**, 321 (1985).

[15]K. M. Ho and K. P. Bohnen, Phys. Rev. Lett. **59**, 1833 (1987).

[16]D. Wolf, H. Jagodzinski, and W. Moritz, Surf. Sci. **77**, 265 (1978).

[17]W. Moritz, H. Jagodzinski, and D. Wolf, Surf. Sci. **77**, 249 (1978).

[18]H. Jagodzinski, W. Moritz, and D. Wolf, Surf. Sci. **77**, 233 (1978).

[19]D. Wolf, H. Hagodzinski, and W. Moritz, Surf. Sci. **77**, 283 (1978).

[20]Y. Kuk, P. J. Silverman, and F. M. Chua, J. Microsc. **152**, 449 (1988).

[21]J. K. Gimzewski, R. Berndt, and R. R. Schlittler, Surf. Sci. **247**, 327 (1991); J. Vac. Sci. Technol. B **9**, 897 (1991).

[22]R. C. Jaklevic and L. Elie, Phys. Rev. Lett. **60**, 120 (1988).

[23]R. Emch, J. Nogami, M. M. Dovek, C. A. Lang, and C. F. Quate, J. Appl. Phys. **65**, 79 (1989).

[24]T.-S. Lin and Y.-W. Chung, Surf. Sci. **207**, 539 (1989).

[25]U. H. Bapst, Surf. Sci. **181**, 157 (1987).

[26]D. W. Abraham, C. C. Williams, and H. K. Wickramasinghe, J. Microsc. **152**, 599 (1988).

[27]E. Stoll and J. K. Gimzewski, J. Vac. Sci. Technol. B **9**, 643 (1991).

[28]J. K. Gimzewski, R. Berndt, and R. R. Schlittler (unpublished).

[29]M. Mundschau, E. Bauer, W. Telieps, and W. Swiech, Surf. Sci. **223**, 413 (1989).

[30]G. Comsa, in *Proceedings of the International School on Material Science and Technology, Erice, Italy, 1981,* edited by G. Benedek and U. Valbusa (Springer, Berlin, 1982).

[31]We thank J. Tersoff for calculating step profiles shown in Fig. 8 using a method described in Ref. 33.

[32]J. Tersoff and D. R. Hamann, Phys. Rev. B **31**, 805 (1985); Phys. Rev. Lett. **50**, 1998 (1983).
[33]M. Sotto and J. C. Bailiard, Surf. Sci. **214**, 97 (1989).
[34]W. J. Kaiser and R. C. Jaklevic, Surf. Sci. **182**, L227 (1987).
[35]K. Takayanagi, Y. Tanishiro, K. Kobayashi, K. Akiyama, and K. Yagi, Jpn. J. Appl. Phys. **26**, L957 (1987).
[36]A. Bartolini, F. Ercolessi, and E. Tosatti, Phys. Rev. Lett. **63**, 872 (1989).
[37]L. D. Roelofs, S. M. Foiles, M. S. Daw, and M. I. Baskes, Surf. Sci. **234**, 63, (1990).
[38]U. Messerschmidt and F. Appel, in *Electron Microscopy in Solid State Physics,* edited by H. Bethge and J. Heydenreich (Elsevier, Amsterdam, 1987), p. 325.
[39]A. Samsavar, E. S. Hirschorn, T. Miller, F. M. Leibsle, J. A. Eades, and T. C. Chiang, Phys. Rev. Lett. **65**, 1907 (1990).
[40]Ion-scattering studies indicate missing atoms are only detected at temperatures above 530 K. See E. van de Riet, H. Derks, and W. Heiland, Surf. Sci. **234**, 53 (1990).
[41]P. Häberle, P. Fenter, and T. Gustafsson, Phys. Rev. B **39**, 5810 (1989).
[42]L. D. Marks, in *Direct Imaging of Atomic Rearrangements on Extended Gold Surfaces,* edited by J. B. Roberto, R. W. Carpenter, and M. C. Wittels, MRS Symposia Proceedings No. 41 (Materials Research Society, Pittsburgh, 1985), p. 129.
[43]J. D. Wrigley and G. Ehrlich, Phys. Rev. Lett. **44**, 661 (1980).
[44]A recent paper on the structure of the Pt(110) and Au(110)(1×2) reconstructed surfaces has been published by T. Gritsh, D. Coulman, R. J. Behm, and G. Ertl, Surf. Sci. **257**, 297 (1991).
[45]Atomic resolution on (111) planes has been reported for several surfaces. See V. M. Hallmark, S. Chiang, J. F. Rabolt, J. D. Swalen, and R. J. Wilson, Phys. Rev. Lett. **59**, 2879 (1987) and J. Wintterlin, J. Wiechers, H. Brune, T. Gritsch, H. Höfer, and R. J. Behm, *ibid.* **62**, 59 (1988).

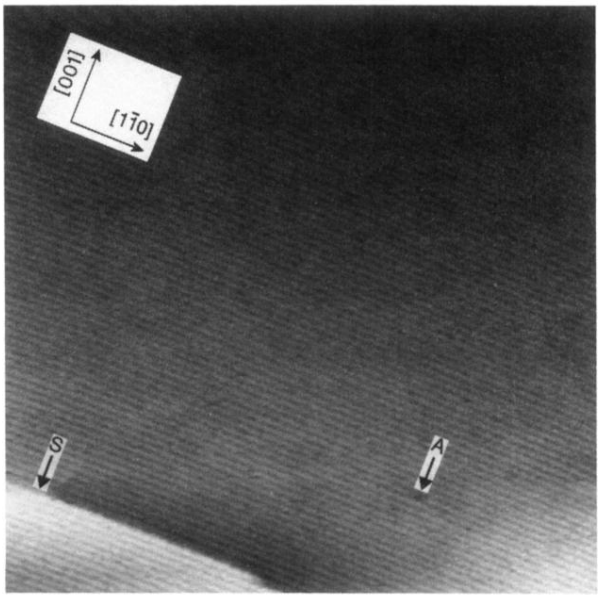

FIG. 1. Gray-scale image of STM topograph from the Au(110) surface exhibiting (1×2) reconstruction. Notice atomic step in bottom left of picture. Area = 670×670 Å^2. V_t=0.37 V, i_t=350 pA.

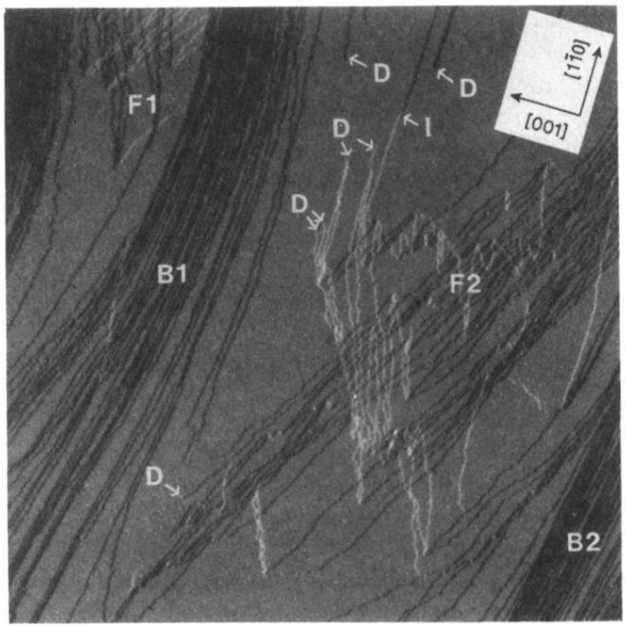

FIG. 10. Gray-scale post-differentiated (dz/dx) image of an STM topograph from a 0.5×0.5-μm^2 area measured at $V_t=0.25$ V, $i_t=200$ pA.

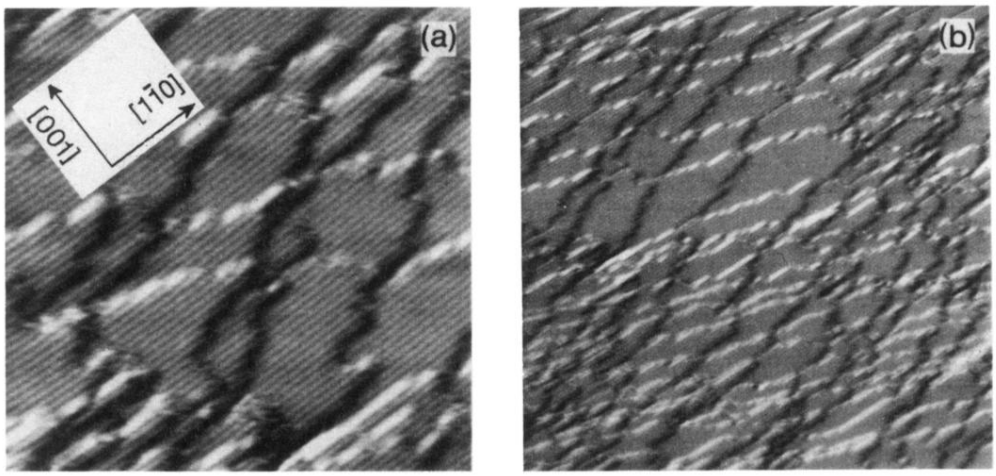

FIG. 11. Gray-scale image of a differential STM topograph from Au(110) showing textured patterns. (a) Area in 550×550 Å^2 and (b) area of 1100×1100 Å^2. Differential topography shows steps as distinct dark or light bands depending on slope sign. $V_t=0.25$ V, $i_t=200$ pA.

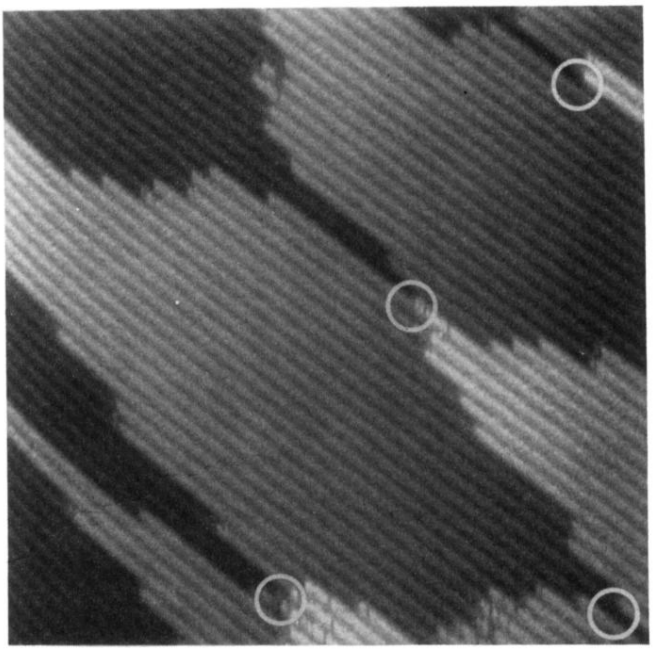

FIG. 12. Detailed gray-scale image of a STM topograph from Au(110) showing steps forming a textured pattern. The (111) steps delineate antiphase domains.

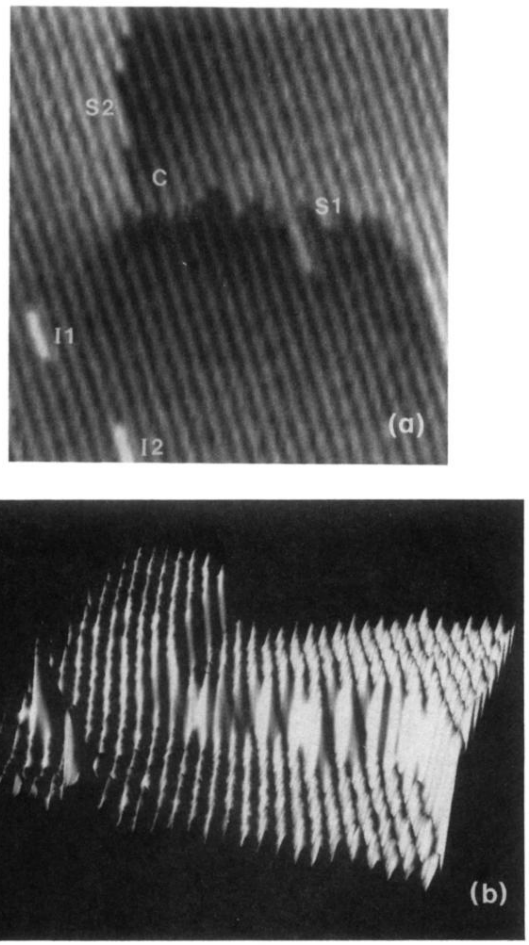

FIG. 13. (a) Gray-scale image of a STM topograph of a dislocation emerging from the surface (see text for explanation of marker). Area $=240\times240$ Å^2, $V_t=0.37$ V, $i_t=200$ pA. (b) Pseudoilluminated 3D representation of (a). Note that filtering was applied in (b) to reduce the corrugation amplitude enabling the dislocation to be better visualized.

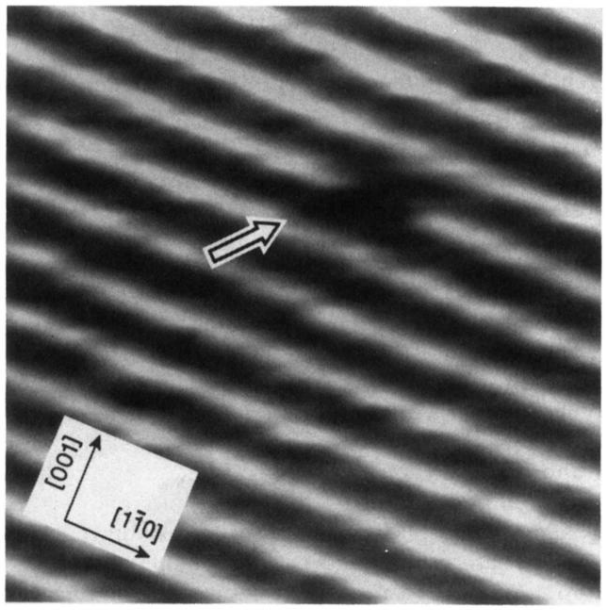

FIG. 14. Gray-scale image of a STM topograph of four missing atoms in a row of the (1×2) reconstruction. $V_t = 0.25$ V, $i_t = 200$ pA.

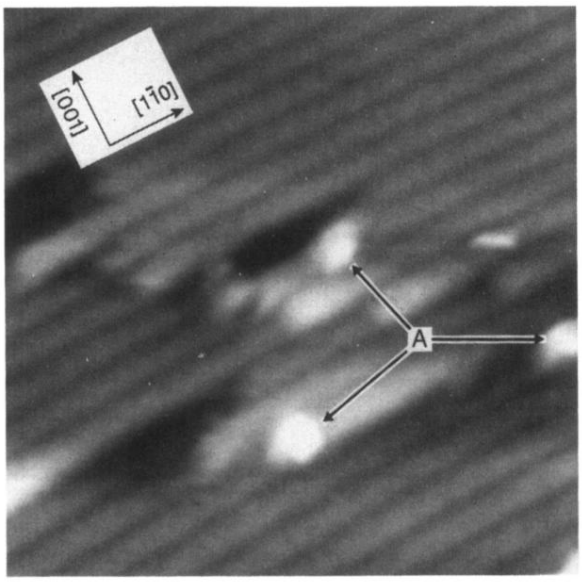

FIG. 15. Gray-scale image of a STM topograph of Au(110) showing three small structures deposited by pulsing the tip at +5 V for 10 ms. The structures are ~3 Å in height and their shape was independent of tip polarity within the range $|V_t| < 1$ V.

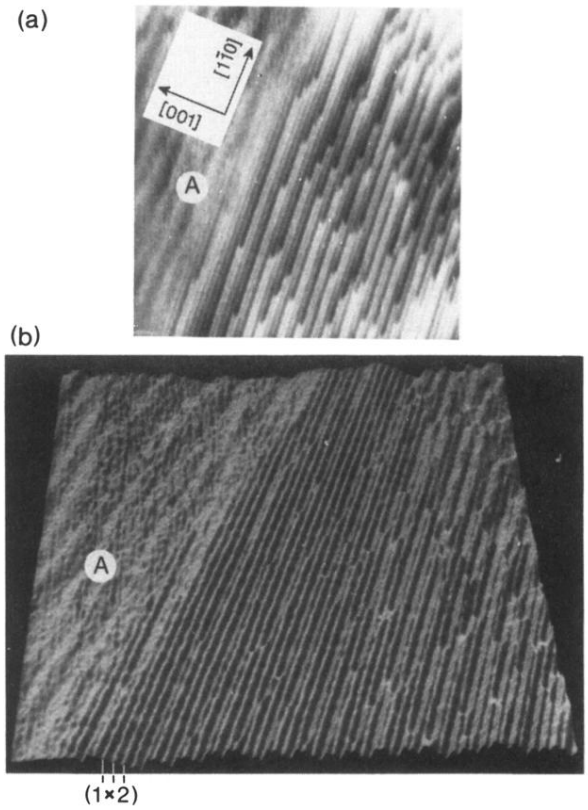

FIG. 16. (a) Gray-scale image of a STM topograph from contaminated Au(110). (b) Pseudoilluminated 3D representation of the same topograph. Area $=500\times500$ Å^2, recorded ~80 h after preparation and left in a UHV at $\rho\sim4\times10^{-10}$ mbar. Topographs of the fresh film were similar to previous figures.

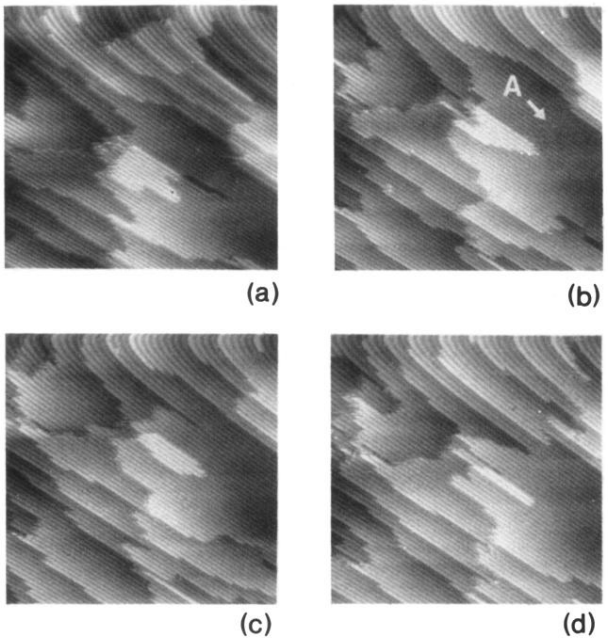

FIG. 17. (a)–(d) Gray-scale images of a 400×400-Å^2 STM topograph of Au(110) recorded at two-hour time intervals. The apparent bending of atomic rows at the tops of the pictures is due to creep of the piezoelectric scanners.

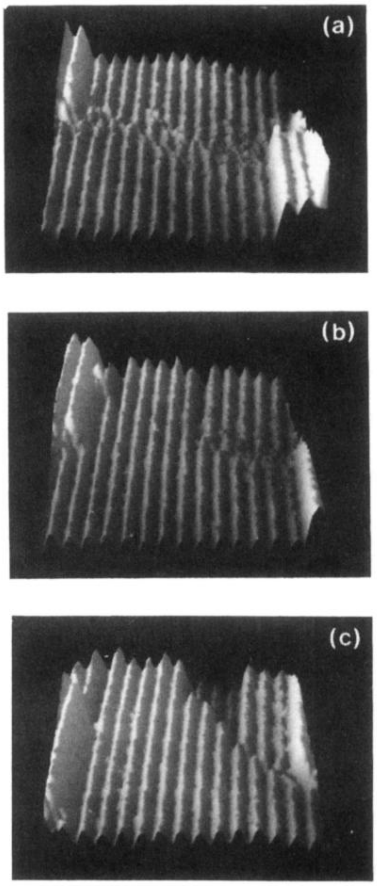

FIG. 18. Pseudoilluminated images of STM topographs of a 120×170-Å^2 area of Au(110) selected from a series recorded at time intervals of 30 min, with $V_t=0.25$ V and $i_t=150$ pA. The surface shows (1×2) reconstruction. Horizontally, a domain boundary separates two (1×2) domains, which are displaced by one lattice constant in the [001] direction. The domain boundary initially extends over eleven (1×2) atomic rows and collapses down to three out of phase rows in the later stages of the measurement. On the time scale of measurement, rows apparently jump instantaneously in a concerted fashion.

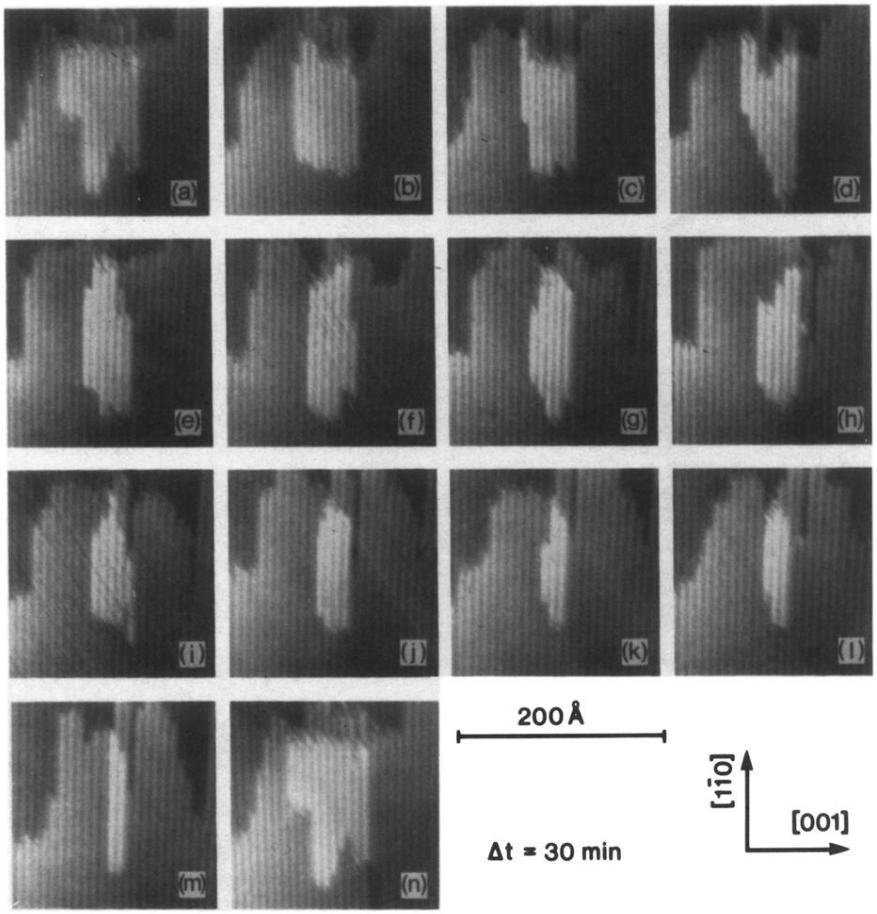

FIG. 19. Sequence of gray-scale images of STM topographs which display structural changes occurring at a (1×2) reconstructed miniterrace. The time interval between each picture is 30 min. Part (n) is a repetition of (e). Over the total measurement time of 6 h the miniterrace gradually dissolves from (d) initially 12 rows to (m) 3 rows.

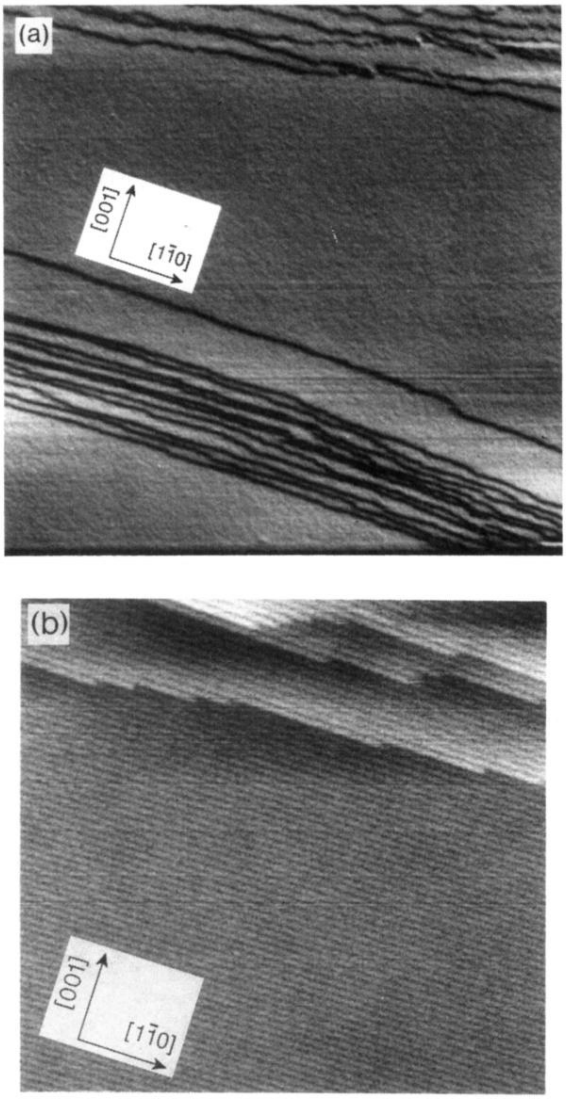

FIG. 2. (a) Pseudoilluminated 3D image of STM topography from the Au(110) surface recorded on a different run from data shown in Fig. 1. Bands of atomic steps are observed in upper- and lower-middle parts of image. Area denotes $=3000\times3000$ Å^2. $V_t=0.78$ V, $i_t=350$ pA. (b) Gray-scale image of an STM topograph from Au(110) recorded in the upper left corner region of (a) showing the (1×2) reconstruction and a cluster of atomic steps at the top of the figure. Area $.=650\times650$ Å^2. $V_t=0.08$ V, $i_t=350$ pA.

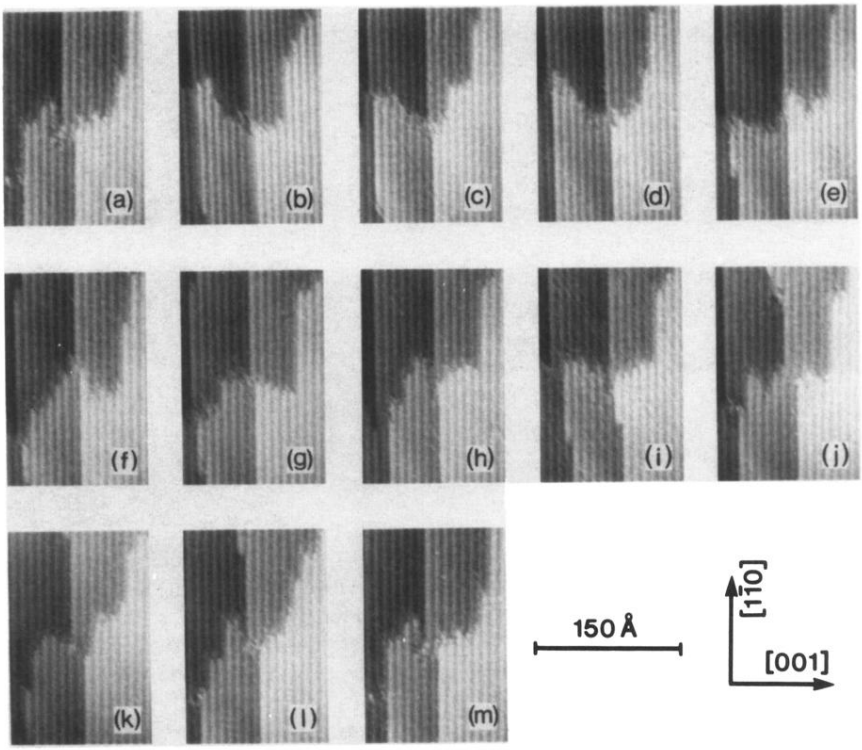

FIG. 20. Time series of gray-scale images of STM topographs recorded every 30 min showing the development of a (1×2) reconstructed area which is divided into three terraces by monatomic steps. The middle and top terrace expose unusually wide steps along the unfavorable [001] direction. These steps meet in all the pictures creating a convenient reference point.

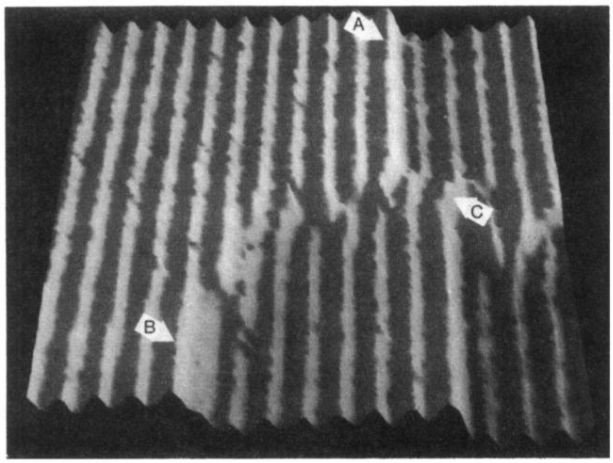

FIG. 21. Detailed pseudoilluminated 3D representation of Fig. 20(a). The atomic rows along the $[1\bar{1}0]$ azimuth are visible on three terraces. The middle terrace consists of two domains separated by a derailment boundary marked C. The displacement by one lattice constant of the underlying gold crystal between these domains forces the topmost terrace to form a (111) microfacet step in the upper part of the surface (A) and a (331) microfacet step in the lower part (B).

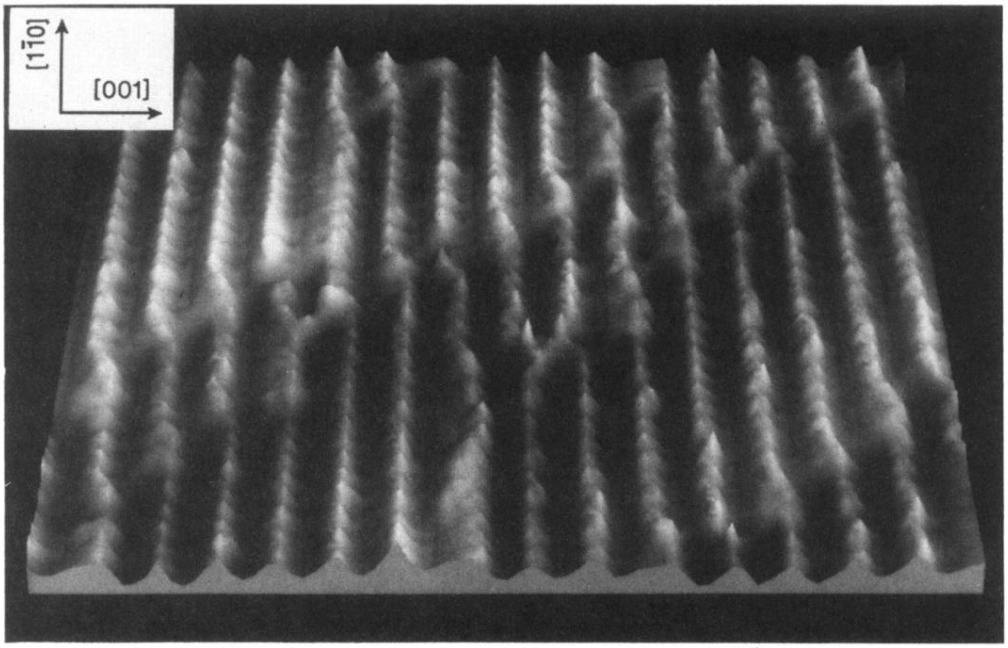

FIG. 22. Pseudoilluminated 3D representation of a topograph from an area (120×90 Å^2) recorded at $i_t = 1$ nA and $V_t = -0.8$ V. Rows along [1$\bar{1}$0] exhibit a corrugation of 0.3 Å with a periodicity of 2.9 Å corresponding to the nearest-neighbor distance of gold.

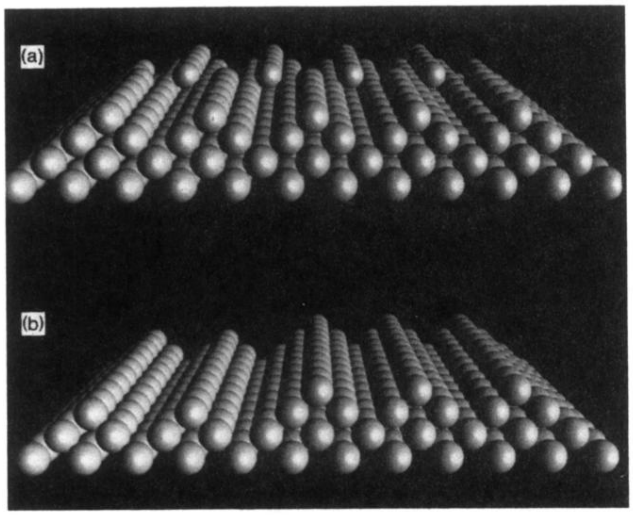

FIG. 3. Models of antiphase boundaries for a Au(110)(1×2) surface proposed by Wolf, Jagodzinski, and Moritz (Ref. 19). (a) Domain boundary formed vertical to ordered chains with not atomic step by a unit-cell displacement in the origin of the superstructure on a flat surface which we call the "derailment wall." (b) Two ordered domains separated by a (111) step generating a displacement of the origin of the superstructure, which we call a "step" wall.

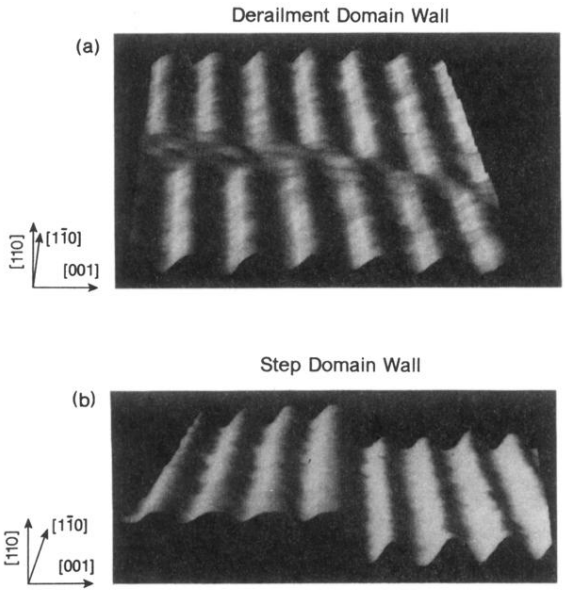

FIG. 4. Pseudoilluminated 3D image of a region of a STM topograph from the Au(110) surface corresponding to the disorder model in Fig. 3. (a) shows the (1×2) two domains displaced by unit cell along the [001] direction displacement forming a derailment domain wall, and (b) shows a domain boundary formed by an additional atomic layer. $V_t=0.25$ V, $i_t=150$ pA.

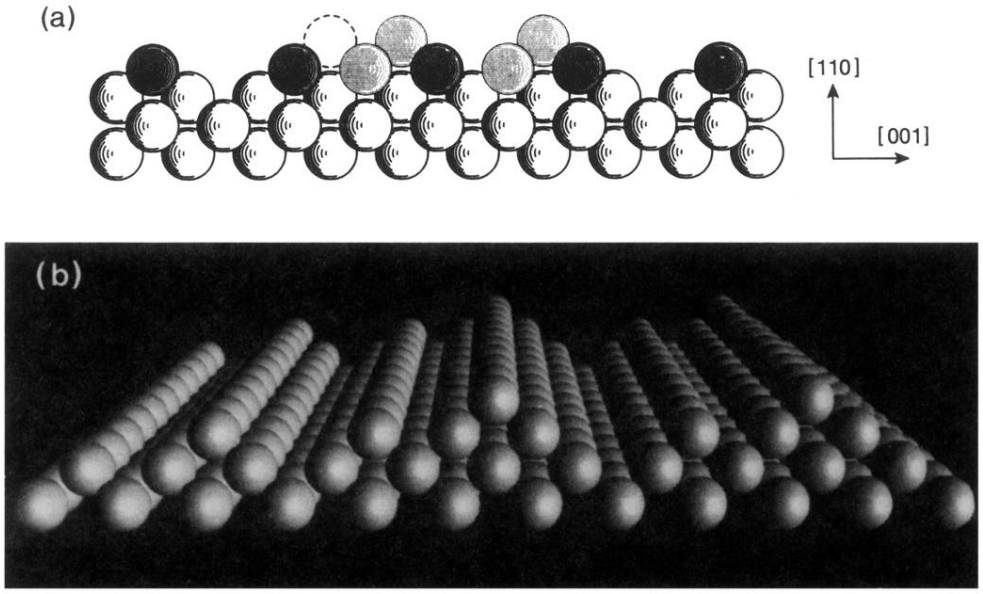

FIG. 5. (a) Schematic illustration of the effect of adding a miniterrace adlayer of Au atoms to a single (1×2) phase. On the left a stable (111) facet may be formed. However, termination of the facet on the right results in a (1×1) row if the hatched atom is present or in a local type (1×3) structure if it is missing. (b) Models of (111) and (331) steps produced by adding additional (1×2) rows to a monophase terrace.

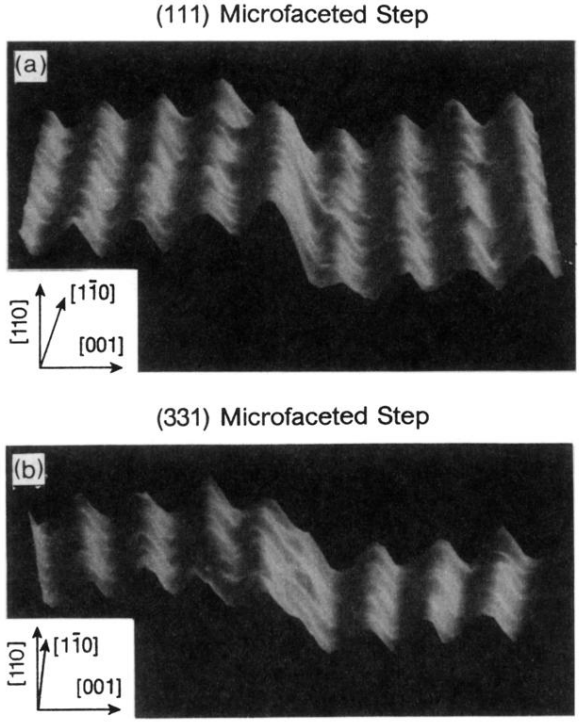

FIG. 6. Pseudoilluminated 3D image of STM images of Au(110)(1×2) showing (a) a step across the [100] direction exposing a (111) microfacet and (b) a step across the [100] direction exposing a (331) microfacet, which is observed only rarely. $V_t = 0.25$ V, $i_t = 150$ pA.

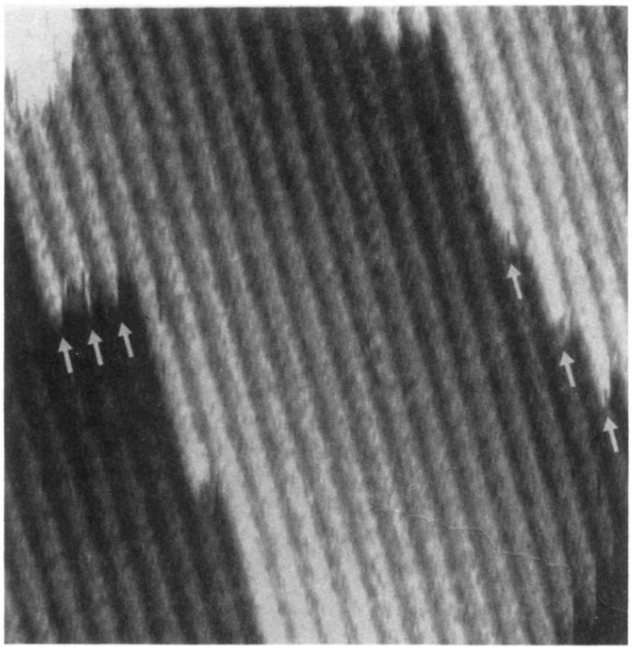

FIG. 9. Detailed gray-scale image of a STM topograph for Au(110) showing a sequence of steps with preferential ordering in the $[1\bar{1}0]$ direction and poor ordering in the [001] direction. Note the apparent lack of resolution on particular kinks (arrows). $V_t = 0.56$ V, $i_t = 200$ pA.